



**POLITECNICO
DI TORINO**

Master's Degree in Mechanical Engineering

Department of Mechanical and Aerospace Engineering

Master's Degree Thesis

Numerical Simulation of a Trapped-vortex Combustor

Supervisors:

Prof. FERLAUTO MICHELE

Prof. ZHU YUEJIN

Candidate:

XIE JIN

July 2020

Abstract

A modified combustor model has been designed in the previous work. The previous work mainly addressed the validation of the priority of the performance of the modified model. The results showed that it is possible to achieve highly effective combustion and lower pressure loss together with low emission of the NO_x. The current research is mainly focusing on the geometrical sizes of the modified combustor model. Different from the previous work, instantaneous cases are studied in this research to go in deep of the formation of the vortex and development of the flow field. Hot and cold cases are discussed to visualize the differences under two conditions. In each group of sizes, detailed advances of the vortices, turbulence kinetic energy and temperature distribution are analyzed. The main conclusions are that the obvious difference between cold and hot cases is that the turbulent energy is higher in reaction case. Besides, the length of the undercut has less effects on the flow and temperature field, but too large size should be avoided taking account that the pressure loss would be increasing significantly if the flow channel is reduced. Then, the value of l/L should not be too small to prevent interference between bevel and rear blunt body. Finally, if the angle, with respect to the horizontal level, is sharp, many times of shedding and generation of vortices would happen.

Key words: Advanced vortex combustor; Variable cross-section; Geometrical parameters; Numerical simulation

List of Figures

Fig. 1. Scheme of the TVC model. -----	8
Fig. 2. Scheme of the AVC model. -----	8
Fig. 3. Geometric model of the original AVC. -----	17
Fig. 4. Temperature distribution of the original model [7]. -----	18
Fig. 5. Geometric model of the modified AVC [28]. -----	18
Fig. 6. Independence test of grid number. -----	19
Fig. 7. Cavity grid distribution. -----	19
Fig. 8. Comparisons of total pressure loss between the numerical and experimental -----	20
Fig. 9. Non-reacting flow field in the original combustor. -----	23
Fig. 10. Development of turbulent kinetic energy. -----	24
Fig. 11. Instantaneous flow field of the modified model under nonreaction. -----	26
Fig. 12. Development of turbulence energy of the modified model under nonreaction. -----	27
Fig. 13. Instantaneous flow field of the modified model under reaction. -----	29
Fig. 14. Development of turbulence energy of the modified model under reaction. -----	30
Fig. 15. Temperature changes with time. -----	31
Fig. 16. Instantaneous development of flow field when the value of C/H is 0.03. -----	33
Fig. 17. Instantaneous development of temperature field when the value of C/H is 0.03. ----	34
Fig. 18. Instantaneous development of flow field when the value of C/H is 0.06. -----	35
Fig. 19. Instantaneous development of temperature field when the value of C/H is 0.06. ----	36
Fig. 20. Development of flow and temperature field when the value of C/H is 0.09. -----	37
Fig. 21. Development of flow and temperature field when the value of C/H is 0.12. -----	38
Fig. 22. Comparison between different groups of l/L at 1ms.-----	39
Fig. 23. Comparison between different groups of l/L at 3ms.-----	40
Fig. 24. Comparison between different groups of l/L at 5ms.-----	41
Fig. 25. Comparison between different groups of l/L at 6ms.-----	42
Fig. 26. Comparison between different groups of l/L at 10ms. -----	43
Fig. 27. Comparison between different groups of l/L at 20ms. -----	44
Fig. 28. Comparison between different groups of l/L at 30ms. -----	45
Fig. 29. Comparison between different groups of l/L at 50ms. -----	46
Fig. 30. Comparison between different time instant when θ is 0° . -----	47
Fig. 31. Comparison between different time instant when θ is 15° .-----	48

Fig. 32. Comparision between different time instant when θ is 30° .----- 49
Fig. 33. Comparision between different time instant when θ is 45° .----- 50
Fig. 34. Comparision between different time instant when θ is 60° .----- 51

List of Tables

Table 1. Parameters that will be analysed.....32

Contents

<i>List of Figures</i>	1
<i>List of Tables</i>	3
<i>Contents</i>	4
1. Introduction	6
2. Numerical model and setup	12
2.1 Numerical method	12
2.2 Turbulence numerical simulation methods	12
2.2.1 DNS.....	13
2.2.2 RANS.....	13
2.2.3 LES	13
2.3 Introduction of OpenFOAM	14
2.4 Procedures to perform OpenFOAM	15
3. Comparisons of two different models	17
3.1. Computational setup	17
3.2. Grid independence validation	19
3.3. Numerical validation	20
3.4 Initial conditions	20
3.5 Results and discussion	21
4. Studies of geometrical parameters of the variable cross-section.	32
4.1 Influence of the value of C/H on the performance.	32
4.2 Influence of the value of l/L on the performance.	38
4.3 Influence of the value of θ on the performance.	47

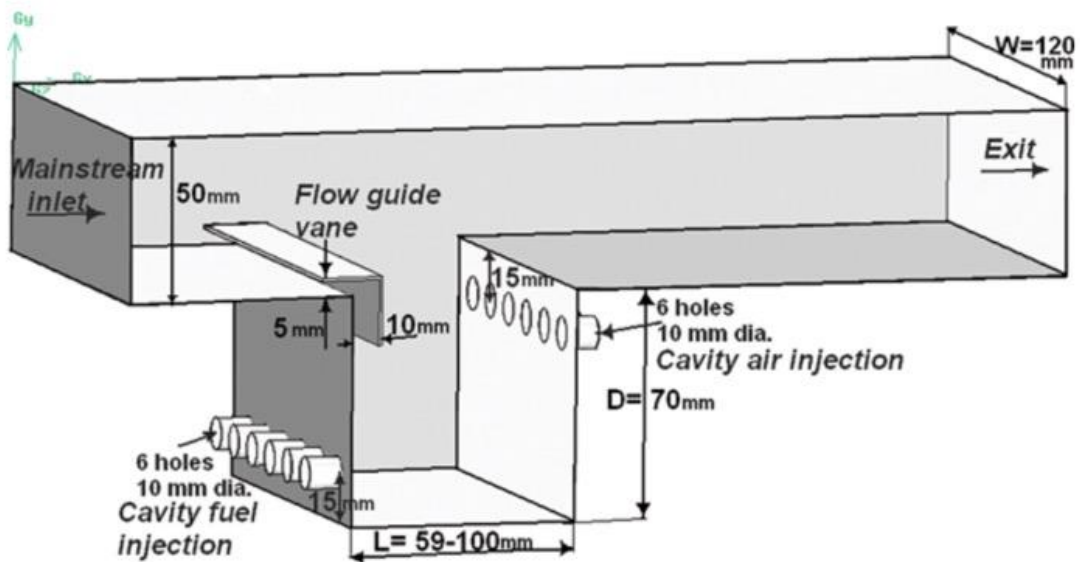
<i>5. Conclusions</i>	52
<i>Acknowledgement</i>	53
<i>Reference</i>	54

1.Introduction

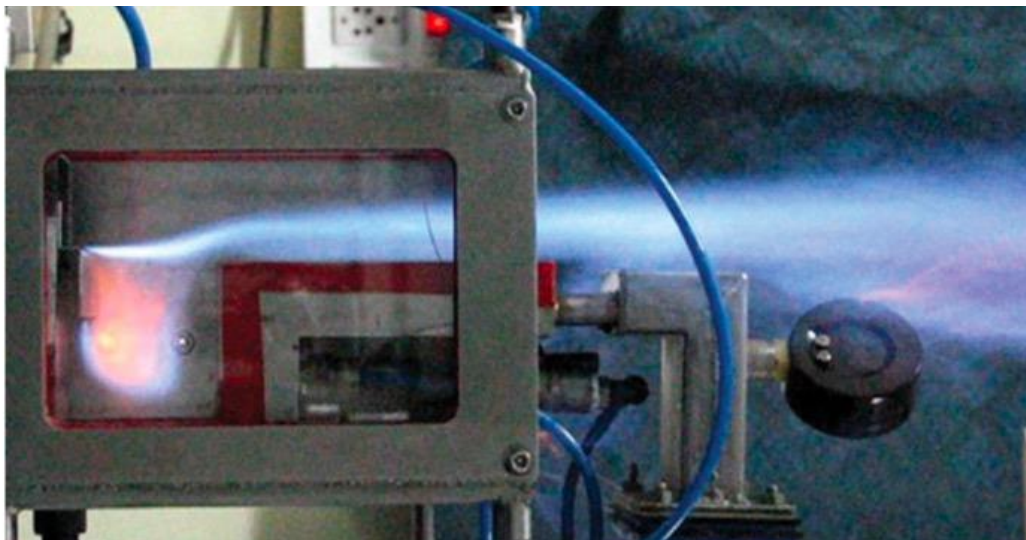
In recent years, with the improvement of living standards, great changes have taken place in people's consumption structure, which has promoted the vigorous development of tourism and stimulated more people to choose convenient, fast and safe air transportation. Therefore, the rapid development of civil aviation industry is particularly important. Although from the perspective of the total emissions of combustion, the share of aero engine emissions is insignificant, but due to its unique local characteristics, and the only source of high-level atmospheric pollutants is generated by aero engines. Near airports, some of the nitrogen oxides emitted by aircraft, ground services, and road traffic are in the form of nitrogen dioxide (NO₂), which can cause breathing problems. Nitrogen oxides emitted from low altitudes are also a key factor in the formation of ground-level ozone (smoke), which may also cause particulate matter formation, reduce visibility and water quality and form acid rain. In addition, nitrogen oxides and unburned hydrocarbons will also undergo photochemical reactions in the atmosphere, generating secondary pollutants and causing greater damage to the environment. As a result, the limits of pollution emission levels of various gas turbines (including aero engines) are becoming stricter. On this basis, it constitutes the need for the development of low-emission aero engines. As an important part of the engine, the combustion chamber should have basic characteristics such as good ignition performance, small total pressure loss, and low pollution emissions. The vortex combustion chamber (TVC) was proposed by the U.S. Air Force Research Office and General Motors in the mid-1990s, and many studies have been carried out to date [1,2]. Compared with conventional swirling combustion chambers, trapped-vortex combustion chambers have attracted widespread attention for their low NO_x emissions, low lean burnout limits, and strong high-altitude re-ignition capabilities.

There are two main kind of combustors that employ cavity to form vortices such that combustors are able to achieve better performance including high fuel combustion efficiency as well as low pollutant emissions. The scheme of the first one is shown in Fig.1 [3], in which up to now has reached the fourth generation. Figure 1(a) is a simplified model for the simulation purpose and (b) is a real product in a test bench. The original purpose of the trapped-vortex combustion chamber was to stabilize the flame and was used to provide the ignition source for the incoming stream. As the research progresses, trapped-vortex combustion chambers have combined a variety of technologies: TVC with guide vanes and blunt bodies, and combustion chambers with stage combustion. TVC with guide vanes and blunt bodies can greatly improve combustion efficiency while reducing emissions. The staged combustion TVC works only in

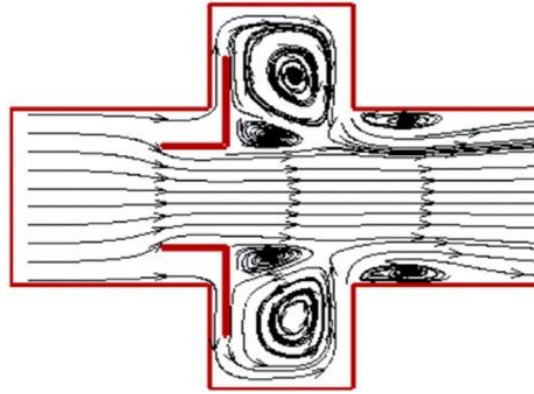
the vortex-holding area at small operating conditions. By injecting fuel into the vortex-holding area for combustion, two vortices, where is demonstrated in (c) [4], can be formed in the cavity and the mainstream inlet does not work, which can reduce emissions while improving working performance. Under heavy working conditions, the mainstream and the vortex region work at the same time, which can obtain a large thrust, and can stabilize the flame and reduce the influence of the mainstream on the flame.



(a) Scheme of the TVC model.



(b) Real model of the TVC model.



(c) Double-vortex structure in the TVC.

Fig. 1. Scheme of the TVC model.

Another one is known as advanced vortex combustor (AVC) [5,6], shown in Fig.2 [7], which is widely used in modern gas turbines and aeroengines to achieve higher combustion efficiency and lower pollution. Although similar to trapped vortex combustors (TVCs), AVCs use blunt bodies instead of cavities, with two independent blunt bodies arranged in the front and rear sections of the combustor. Fuel is injected from an upstream diffuser, which leads to the fuel being mixed with air before entering the combustor. When the incoming flow passes through the front bluff body, a stable vortex structure is formed at the concave cavity between the front and rear bluff bodies, and this acts as a stable ignition source for the combustion chamber. Although there have been numerous studies on TVCs, there has been relatively little research on AVCs, despite them having a simpler structure, higher combustion efficiency, and lower emissions. Hence, it is important to study AVCs in greater detail.

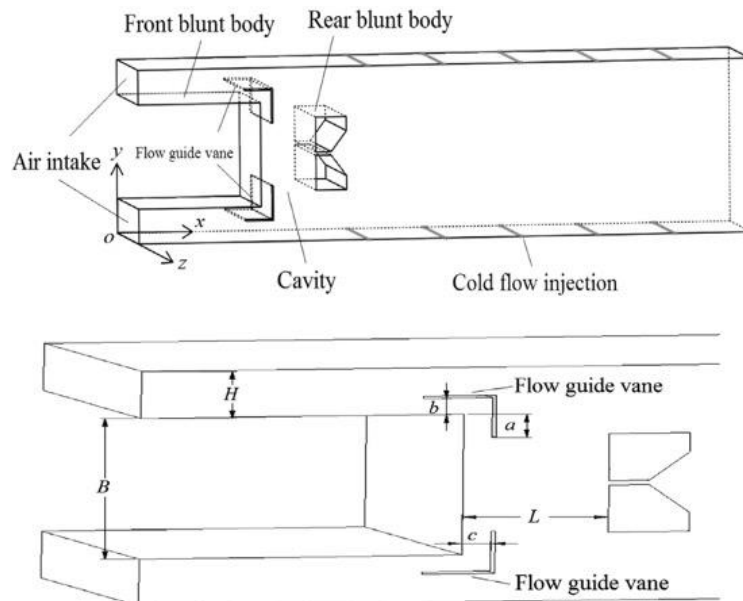


Fig. 2. Scheme of the AVC model.

About the studies of TVC, Hsu et al. [8] first identified its characteristics and it was shown that the trapped vortices in the cavity can provide flame stability and combustion efficiency can be improved. Stone and Menon [9] numerically simulated the fuel-air mixing characteristics of TVC under cold(non-reactive) and reaction conditions, while Selvaganesh and Vengadesan [10] numerically simulated the flow field under cold conditions and determined the best cavity size. Then Ghenai et al. [11] studied the combustion performance and emissions of TVC with two cavities supplying syngas fuels. They revealed that fuels with higher fraction of hydrogen show better performance and it was found that there is a transition of flame location when the fuel is changed. In 2011, Agarwal and Ravikrishna [12] proposed the concept of using guide vanes based on the original TVC. This not only produces a stable double vortex structure in the cavity, but also improves combustion efficiency. Kumar and Mishra [13] presented numerical study for the influence of momentum flux ratio (MFR) on the structure of flame and flow inside a TVC cavity. They concluded that MFR has an evident effect on flow and flame formation and development. Agarwal et al. [3] placed inclined vanes in the guide vanes and experimentally investigated their influence on the mixing condition between fuel and air. It was revealed that they can promote the mixing rate while keep low pressure loss and high combustion efficiency. Zeng et al. [4] added a central blunt body to the TVC with guide vanes to enhance heat and mass exchange in the combustor and further improve combustion efficiency. Wu et al. [14] designed a kind of TVC with interchangeable aerodynamic multi-point fueling (AMF) setups and their experiment operating in nonreacting condition indicates that slender struts are hard to protect vortices so that the cavity flow is hard to reach the tail of the blunt body. In the same year, they [15] used the same device to study how efficiency and pollutant emissions are affected by the width of the struts and fueling conditions. The results demonstrated that cavity-fueling could lead to low combustion efficiency, while main-fueling could improve combustion efficiency and reduce emissions of CO and UHC. Kumar et al. [16] experimentally investigated a 2-D TVC regarding 3 parameters, pollution emissions, combustion efficiency and exit temperature distribution respectively. The results show that mainstream Reynolds number, cavity equivalence ratio, and primary air velocity have obvious influence on the performance of TVC, also they indicated that the flame inside the cavity may suffer quenching if mainstream Reynolds number is in a specific range. Vengadesan and Sony [17] performed a numerical simulation of a TVC with a second cavity and found that the second cavity stabilized combustion. This provides ideas for AVC with dual or multiple chambers. Krishna and Ravikrishna [18] reported the simulation and experimental measurements of temperature distribution and pollutants emissions in a TVC for power generation. In terms of simulation,

they employed both Reynolds-averaged Navier–Stokes (RANS) and large eddy simulations (LES) models, and it was found that LES can achieve high accuracy with respect to measured results. Li et al. [19] experimentally studied the effects of three different combustor dome structures in terms of combustion efficiency, ignition and lean blowout limits. The results indicate that fairing-tube configuration performs well in terms of lean blowout limits and the outer-cavity ignition performance, but fairing-plate structure shows better inner-cavity ignition performance. Li et al. [20] designed a novel hybrid-atomizer used for the supply of fuel and compared its performance with pressure-swirl atomizer. They revealed that the novel atomizer could provide advantages in terms of ignition and combustion efficiency. Zhao et al. [21] reviewed the fundamentals and development of trapped vortex combustor. Then, they described the working principles and applications of TVC in the field of aero engines and power generation. Finally, the outlook of TVC's future and challenge was introduced. Li et al. [22] studied the performance of TVC under different support settings and showed that the support length significantly affected the combustion efficiency. Zhu et al. [23] experimentally and numerically studied how the angle and location of primary injection affect the structure of vortices inside the cavity. It was found that the location of the primary injection has a significant influence on the flow structure. Ghenai [24] conducted numerical studies on the emissions and flame temperatures when supplying hydrogen and syngas fuels. The results show that hydrogen can achieve higher combustion temperature and biohythane is able to produce less CO₂ compared with methane. Some useful conclusions from TVC research can be used in the research and improvement of AVC.

For the research of AVC, Edmonds et al. [6] Proposed and examined a new AVC in which the emissions of pollutant are low. The results reveal that the oscillation of the flame is not obvious and the AVC has the feature that the pressure loss is low. Deng et al. [25] conducted numerically study of the combustion performance when the fuel of the AVC is H₂. The research shows that total pressure loss and completion of the combustion of the fuel are obviously affected by the equivalent ratio of hydrogen to air. Then, they [26] devised an AVC whose shape is circular, and it has three individual blunt bodies mounted in parallel, and they performed numerical and experimental studies of the flow condition, combustion stability, and emissions of pollutant of the AVC. The studies show that the usage of the rear blunt body is able to decrease the flow resistance of the fluid. Zeng et al. [7] applied guide vanes to AVC, and numerically determined the best matching of the parameters of the guide vanes. The results show that when the guide vanes are employed, the double-vortex structure can be easily formed as well. Zeng et al. [27] introduced a slot in the rear blunt body and studied the influence of the

sizes of the slot on the performance of the AVC. The results show that the performance of the AVC reaches the best when the matching of the slot size and opening angle are determined. Xie and Zhu [28] proposed a modified AVC configuration, changing the external structure of the combustor and performed numerical investigation on its performance compared with other TVC models. It was shown that the proposed model has advantages in terms of pollutants emissions, pressure drop and combustion efficiency.

The unsteady situation, however, have not been investigated regarding the newly proposed AVC. The present work will carry out transient numerical simulation in terms of both nonreacting and reacting conditions to study how the vortices form and develop. In addition, parameters of the variable cross-section including distance between inlet and cross-section, the value of the angle of the cross-section and the depth of the cross-section will be investigated numerically to find out the optimal size that can achieve best performance.

This work will be done in four main parts. The first part is an overview of the previous researches relevant to my work and introduction of the motivation and goals of my proposal. In the second chapter are introduced the numerical methods, simulation methods for dealing with turbulence and software for performing the simulation in this work, which is OpenFOAM. In the third chapter, a comparison between the original combustor model and modified model is made to demonstrate the superiorities of the modified model. Transient results will be analyzed for the purpose of observing the development of the key vortices in two different structures.

Finally, due to the geometrical sizes of the variable cross-section have influence on the performance of the combustor, so detailed discussion about them is performed in the fourth chapter. The effects of different values of C/H , l/L and θ are analyzed.

2. Numerical model and setup

2.1 Numerical method

The fluid flow process is restricted by the relevant physical conservation laws. The basic conservation laws are continuity, momentum conservation, energy conservation, etc. If there are different degrees of mixing in the flow or interactions between the fluids, the system must be controlled by the law of conservation of components. If the flow is in a turbulent state, the system must also obey additional turbulent transport equations. In the present study, we treat our flow is turbulent and incompressible, so the corresponding Navier-Stokes (N-S) equations can be written as follows:

Continuity:

$$\frac{\partial \rho}{\partial t} + \frac{\partial(\rho u_i)}{\partial x_i} = 0 \quad (1)$$

Momentum conservation:

$$\frac{\partial(\rho u_i u_j)}{\partial x_j} + \frac{\partial(\rho u)}{\partial t} = -\frac{\partial P}{\partial x_i} + \frac{\partial \tau_{ij}}{\partial x_j} \quad (2)$$

Energy conservation:

$$\frac{\partial E}{\partial t} + \frac{\partial}{\partial x_j} (u_j E + p u_j) = -\frac{\partial q_j}{\partial x_j} + \frac{\partial(u_i \tau_{ij})}{\partial x_j} \quad (3)$$

Components conservation:

$$\frac{\partial}{\partial x_j} (\rho S u_j) = \frac{\partial}{\partial t} \left(D \rho \frac{\partial S}{\partial x_j} \right) - \rho \dot{\omega} \quad (4)$$

Where ρ is the density of the fluid, u_i represents the velocity component of the gas in the i direction, P represents the pressure of the fluid, τ_{ij} is the viscous stress tensor. E is the total energy per volume, S is the mass fraction of the involved species of the chemical reaction, D is the coefficient of diffusion, and $\dot{\omega}$ is the chemical reactive rate.

k - ε turbulence model is used.

2.2 Turbulence numerical simulation methods

Turbulent numerical simulation methods are divided into direct numerical simulation and indirect numerical simulation. The direct numerical simulation is to directly solve the instantaneous flow control equation. Instead, direct numerical simulation is to find a way to simplify the turbulence and obtain a numerical solution that is very close to the actual flow condition. According to different simplified methods adopted, indirect numerical simulation methods can be divided into Reynolds average numerical simulation (RANS) method, large eddy simulation (LES), detached eddy simulation (DES) and other methods.

2.2.1 DNS

Direct numerical simulation method is to directly calculate the turbulent flow to solve the instantaneous process. Because it is a direct solution to the governing equations, the numerical results obtained by this method are the closest to the actual flow variables. However, due to the complexity and irregularity of turbulent motion, very small spatial grid scales and time steps are required to solve the results accurately, which makes the implementation of direct numerical simulation methods require huge computer resources. However, as far as the current level of computer development is concerned, direct numerical simulation of all turbulent motions cannot be performed. Direct numerical simulation can only be performed for flows with low turbulent Reynolds numbers and very simple geometric models. However, it cannot be denied that the direct numerical simulation method is an effective tool to study the turbulence mechanism and it is very likely that this method will be widely applied to practical engineering calculations in the near future with the advances of the computer level.

2.2.2 RANS

As mentioned above, although the direct solution of the instantaneous equation can obtain accurate numerical solutions, the limitation of the development of the computer and the nonlinear terms in the control equation increase the difficulty of numerical solution, so that the analytical method is used to accurately describe all the details of the three-dimensional flow field that related time are extremely difficult. In order to solve this problem, researchers have discovered that although the details of the turbulent pulsation change irregularly in space and time during the study of the flow phenomenon, these detail variables meet the statistical average characteristics. Earlier we mentioned that N-S equations accurately describes the phenomenon of turbulent motion, then the statistical averaging of the N-S equations can describe the change of turbulent statistics. The Reynolds average method is a statistical averaging method that performs time averaging on the N-S equations. The Reynolds average method reflects the role of transient pulsation in the flow by establishing a model. Its core is to reduce the amount of calculation by solving the time-averaged N-S.

2.2.3 LES

LES is a method of spatial averaging of N-S equations. The LES theory holds that large-scale pulsations in the turbulent flow contain the main energy and momentum and dominate the momentum and energy transport of the turbulent flow pulsations; while small-scale pulsations are the areas where the kinetic energy of turbulent flow is dissipated. The principle of LES is

performing direct numerical simulation for the large-scale turbulent flow and performing the sub-lattice scale model to simulate the impact of small-scale pulsations on the flow field. In the case of using a suitable sub-grid scale model, the large eddy simulation results have higher accuracy and less calculation workload, and the simulation results are closed to real transient flow.

LES method was originally developed by meteorologists to predict weather conditions. In the area far from the surface, the research field can be regarded as unbounded, and the scale of the vortices in the air is generally very large. LES can be used to the calculation so that the size of the grids can be set to a larger size. However, in realistic complex models, especially geometric models with wall boundary layers, the use of LES is quite computationally expensive. This is because the scale of the vortex structure near the boundary layer is very small. To obtain the turbulent flow information near the wall surface, the grid near the wall surface needs to be meshed very thin, so applying the LES will consume a lot of computing resources.

2.3 Introduction of OpenFOAM

OpenFOAM is a fully functional CFD open source toolbox developed by OpenCFD Co., Ltd. It is also a collection of C++ libraries and executable files that follow a highly modular and object-oriented programming method. It provides extensive functional support in all aspects of fluid flow and heat transfer. In addition to about 80 built-in connectors, it also includes more than 170 pre-processing, post-processing, visualization and other tools. Besides being freely available to any user, the biggest advantage of OpenFOAM is that its source code is also free and open. This makes it very attractive for both academics and commercial software users. OpenFOAM is released under the GNU GPL license, which allows users to modify and compile the source code according to their actual needs.

Some features of OpenFOAM include:

- Solve different types of problems: incompressible, compressible flow problems, buoyancy, multiphase flow, chemical reaction flow, etc.
- Provide a variety of numerical formats and boundary conditions.
- Tightly integrated with Paraview, where Paraview is an open source tool that can directly postprocess OpenFOAM results.
- Support a variety of grid conversion tools and can convert a variety of popular commercial grid format into OpenFOAM grid; and with a variety of tools, it can convert

simulation data into common commercial formats, such as IGES, STP and other standard formats.

- The parallel processing performance is robust, and the linear expansion performance is up to 1000 cores.
- Highly vectorized and templated C++ code, coding style focusing on operation speed and performance

2.4 Procedures to perform OpenFOAM

- Problem definition and planning

Usually CFD is used to solve engineering flow problems, and the simulation software is not used from the beginning, unless the details of the problem that need to be solved is very clear. In general, before performing CFD calculations, it is needed to carefully analyze the physical problems involved, such as which physical models are involved in the calculation, whether the flow is laminar or turbulent, which physical quantities are to be calculated, what calculation domain is used, and can the computing domain be simplified, etc.

- Computational area geometry construction

Based on a careful analysis of the problem, it is time to start thinking about constructing a computing area. In the process of constructing the calculation area, it is necessary to consider: can the calculation area use symmetry or periodic conditions? Is it possible to use 2D models? Can some small features be simplified? Does the calculation domain contain motion areas? etc. After the model is planned, the model can be created. There are many tools for creating geometric models, some of which use external CAD software, and some CAE pre-processing software have certain geometry creation functions. But no matter which way is used to create the geometry, it is finally necessary to divide these geometric models into computing grids. Therefore, when creating geometric models, it should also consider the meshing software used later.

- Computational meshing

Grid division has always been a hot topic in the CFD calculation process and the role of the grid in the calculation process is indeed very important, which affects the calculation accuracy and convergence. In the process of CFD application, professional grid generation tools can be used to create grids.

- Numerical model selection and parameter setting

What kind of numerical model to choose is generally determined during the problem planning process, but the model-related parameters need to be set after the model selection. Different physical models involve different parameters, so it is necessary to understand the mathematical physics behind the physical model in order to do an accurate simulation.

- Physical parameter setting

The needs to specify which physical properties are sometimes related to the physical model. Usually for pure flow problems, there is only needs to specify the viscosity and density of the fluid; if heat transfer is involved, we need to specify the specific heat and the coefficient of thermal expansion.

- Designation of boundary conditions and initial conditions

They are very important contents, usually determines the correctness of the calculation result directly, and often affects the convergence and stability of the calculation. It needs to be set according to the actual situation.

- Discrete algorithm specification

It determines the accuracy of calculation and the speed of convergence.

- Calculation control parameter specification

Such as the specification of the residual standard, the number of iterations, the time step, etc. After the above steps are completed, the solver can be started to perform iterative calculations. Then the Post-processing after calculation is followed.

In this chapter, control equations and turbulence numerical simulation methods are introduced and some brief discussion of OpenFOAM also is shown. Because the practicability of our simulation is strictly dependent on the selection of numerical method, so properly choosing numerical methods is important to get realistic results.

3. Comparisons of two different models

3.1. Computational setup

Figure 3 shows the original model of advanced vortex combustor, which is composed of main flow channel and two blunt bodies mounted in the front and rear part of the channel, therefore a cavity in between is automatically formed. W_1 and W_2 are the width of the front and rear blunt bodies, respectively. H_1 and H_2 are the height of them. L_1 and L_2 are the length of them. S is the distance between them. The advantages of the aforementioned design are mainly that when the incoming flow passes through the front bluff body, a stable vortex structure is formed in the cavity between the front and rear bluff bodies, which serves as a stable ignition source for the combustion chamber; on the other hand, the presence of a stable vortex can not only effectively reduce the combustion chamber total pressure loss and pollutant emissions, combustion efficiency can also be greatly improved.

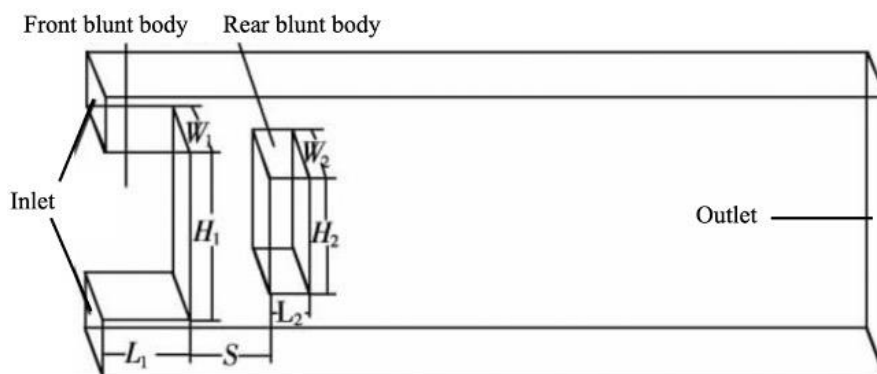


Fig. 3. Geometric model of the original AVC.

However, based on the existing researches, in the original model, the fuel is not completely exhausted especially near the upper and lower walls resulting to the waste of fuel and the decrease of combustion efficiency. This case can be shown in Fig.4. In the upper case, guide vanes are employed, and we can see that the uniformity of temperature distribution is enhanced but the low temperature feature can also be evidenced near the walls even with the addition of the guide vanes.

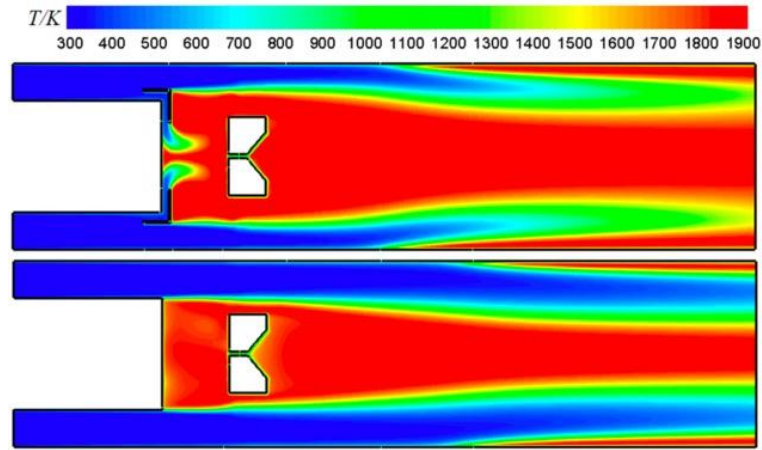
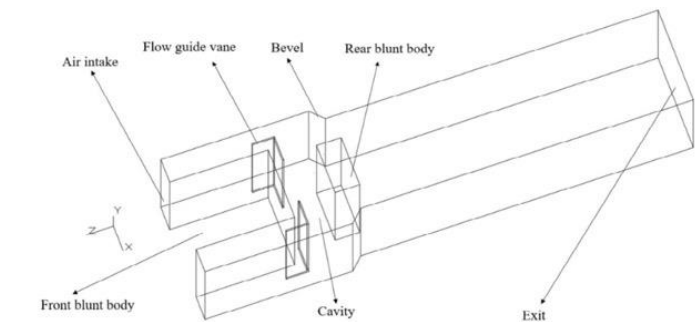
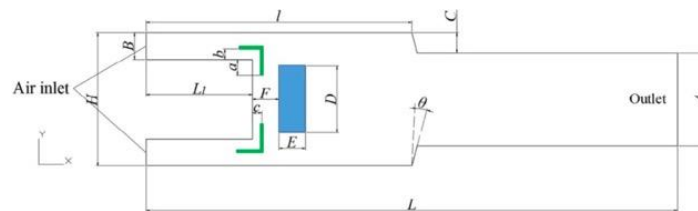


Fig. 4. Temperature distribution of the original model [7].

Depicted in Fig.5 is the modified configuration. The size of combustor channel is $400 \text{ mm} \times 100 \text{ mm}$, the front blunt body is $80 \text{ mm} \times 60 \text{ mm}$, θ is the angle between the bevel of variable cross-section and the vertical position, E is the length of the bluff body, l is the distance from the bevel to the inlet, A and D are the height of the bluff body and the outlet respectively. The proved guide vanes and blunt body parameters in [7] are utilized as the structural parameters, in which the relationships of them are $a/H=0.2$, $b/B=0.4$, $c/F=0.1$ and the size of the rear blunt body is $E \times D=20 \text{ mm} \times 42 \text{ mm}$. The aim of this proposal is to improve the blending of the flow inside the cavity by means of the design of variable cross-section. When the flow is crossing the cavity, due to the influence of the reduced cross-section, the flow near the walls can have a good mixing condition and therefore improving combustion.



(a) 3D sketch of the combustor construction



(b) 2D sketch of the combustor construction

Fig. 5. Geometric model of the modified AVC [28].

3.2. Grid independence validation

Grid independence verification is an important aspect to evaluate the validity of numerical calculation results. In this case, in order to study the influence of grid number on the calculation results, the combustion flow simulation of AVC under two grid numbers is carried out. The calculation results are shown in Fig.6, where the number of grids of (a) is about 80,000, and (b) is the combustion flow field when the number of grids is about 160,000. It can be seen that when the grid number is doubled, the calculation results are not significantly different, thus verifying the grid independence. In order to reduce the calculation workload, the number of grid cells in the calculation is controlled at about 80,000. The grid distribution of the combustor cavity region is shown in Fig. 7.

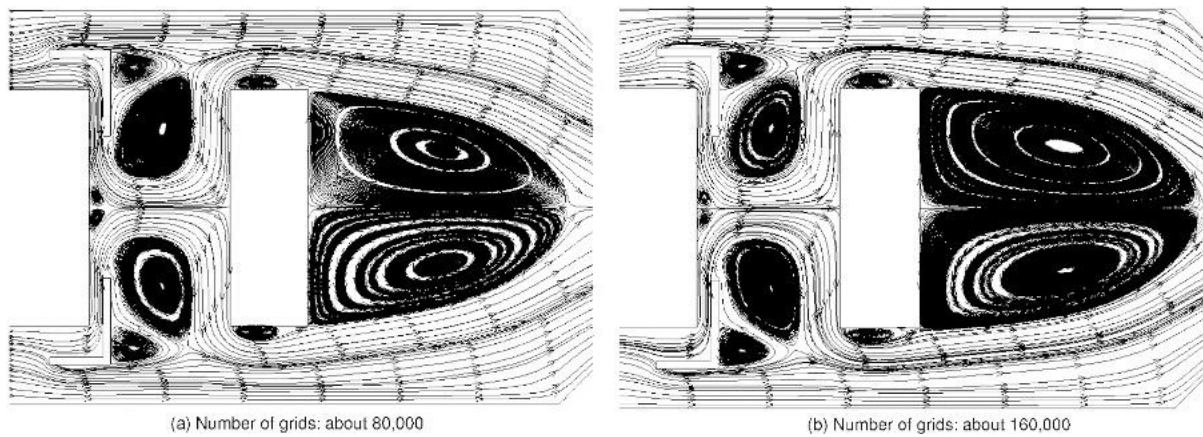


Fig. 6. Independence test of grid number.

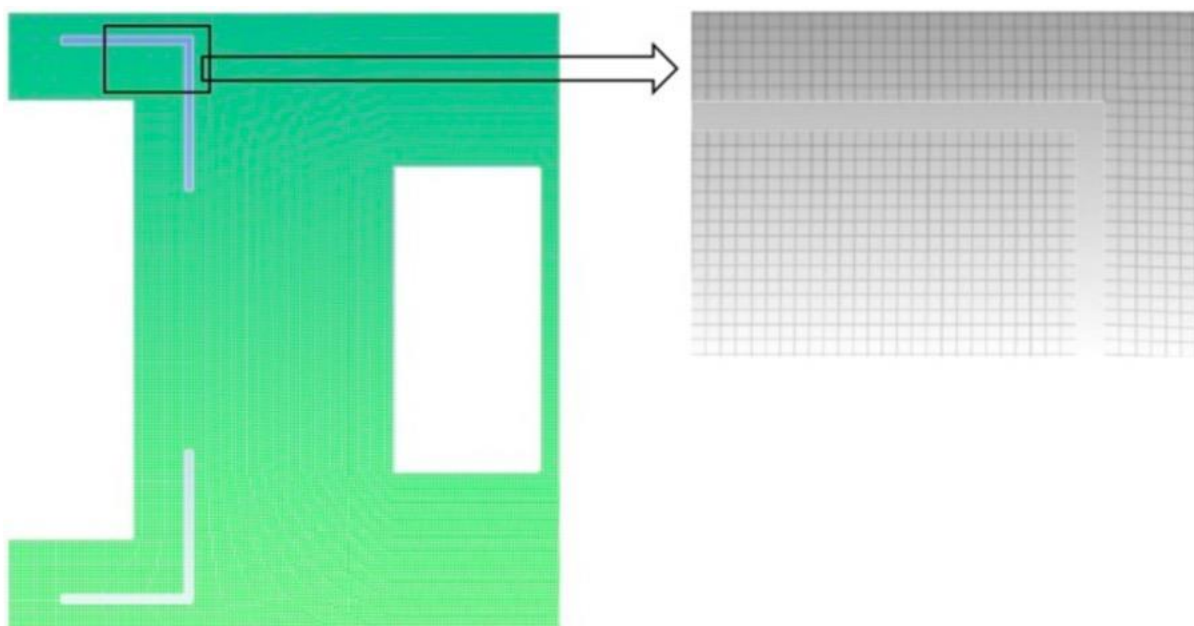


Fig. 7. Cavity grid distribution.

3.3. Numerical validation

The total pressure loss coefficient is defined as follows:

$$\delta^* = \frac{P_1^* - P_2^*}{P_1^*} \quad (5)$$

where P_1^* and P_2^* are the total pressure of inlet and outlet, respectively. According to this, Fig. 8 shows the comparisons of total pressure loss between the numerical and experimental results [8] when $b/B = 0.1$. It is easy to find that the numerical results are in good agreement with the experimental results even they are not perfectly the same. The changing trends of them are alike, which implies that the adopted numerical method in our work are acceptable and reliable.

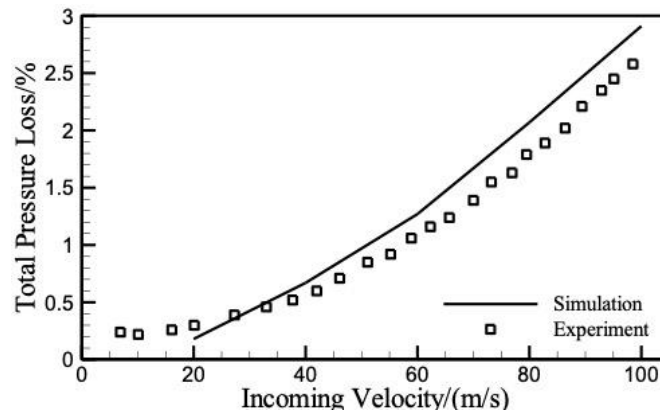


Fig. 8. Comparisons of total pressure loss between the numerical and experimental

3.4 Initial conditions

For the computation of the simulation, correct settings of initial conditions are of great importance. In the '0' folder contains all the initial conditions that need we properly set. Main parameters of them can be approximated in the following,

$$k = \frac{3}{2} * (u_{avg} * I) \quad (6)$$

Where u_{avg} is the average velocity and I is the turbulent intensity which can be approximated by $I = 0.16 * Re^{-\frac{1}{8}}$, Re is the Reynolds number, which can be computed by $Re = \frac{\rho v d}{\mu}$. Where ρ is fluid density, v is the velocity of the fluids, d is the hydraulic diameter, μ is dynamic viscosity of the fluids.

$$\varepsilon = C_{\mu}^{\frac{3}{4}} * \frac{k^{\frac{3}{2}}}{l} \quad (7)$$

Where C_{μ} is constant which can be 0.09 in this case and l is the characteristic length.

$$v_t = \rho * \frac{k}{\omega} \quad (8)$$

Where ρ is fluid density and ω is specific dissipation rate which can be got by $\omega = \frac{k^{\frac{1}{2}}}{C_{\mu}^{\frac{1}{4}} * l}$

3.5 Results and discussion

In order to show the difference between the modified combustion chamber and the original combustion chamber, in the following section, we numerically study the cold state and combustion situation of the two models to find out the flow field development and turbulent kinetic energy distribution.

In Fig.9 shows the non-reacting flow field in the original combustor. At the beginning of the simulation such as 1ms, the flow field is not fully developed and double-vortex structure in the cavity is not formed. But we can evidence the presence of the double-vortex at 3ms, in which the outer vortex is conducive to sucking the external fuel into the cavity for combustion, and at the same time transferring the high-temperature products and heat in the cavity to the mainstream, and playing a role in the heat and mass exchange between the mainstream and the cavity. Due to the shielding of the outer vortex, the internal vortex is not affected by the direct action of the mainstream, so that stable combustion can be achieved, and the symmetry of the inner vortex is the key to the flame stability. In addition, the couple of small vortices in the upper and lower section of the rear blunt body are not obviously evidenced at the beginning. With the advance of time, the main vortex behind rear blunt body is growing towards the outlet along mainstream. From 3ms to 5ms, the vortex continues becoming longer, but from 5ms to 7ms, the length of main vortex has been reduced. At 7ms, internal flow field is almost to be symmetric but the area near the outlet is slightly asymmetric. Main vortex is fully developed, and double-vortex structure is formed, in which can stabilize combustion. At time instant 10ms, 30ms and 50ms, the flow fields of them are almost the same, which means the flow has reached to be steady state. Generally, the flow reaches stable at time instant about 10ms.

From Fig. 10, development of turbulent kinetic energy is depicted. Turbulent kinetic energy is an important characteristic quantity describing the turbulent motion characteristics, and from Equation (6) we can conclude that turbulent kinetic energy is closely related to the turbulent intensity. As we can see, the turbulent kinetic energy is symmetrically distributed at any time instant. When the simulation starts, the higher turbulent kinetic energy is mainly distributed inside the cavity and near the rear blunt body. At 1ms, a core of higher turbulent kinetic energy is formed behind the blunt body, but it disappears with the time increasing due to the

development of the flow field. Besides, higher turbulent kinetic energy moves from the front part to the rear part if the computations continue. At 3ms, the higher turbulent kinetic energy previously appearing inside the cavity is almost vanishing and from 5ms to 7ms, turbulent kinetic energy looks not very concentrated and tends to spread in the combustor. At time instant 7ms, the turbulent kinetic energy in the combustor is almost distributed uniformly but the section near the rear blunt body is an exception due to the exchange of mass and heat happens there. In steady state, contrary to the beginning, the turbulent kinetic energy inside the cavity becomes very small, which means the low disorder.

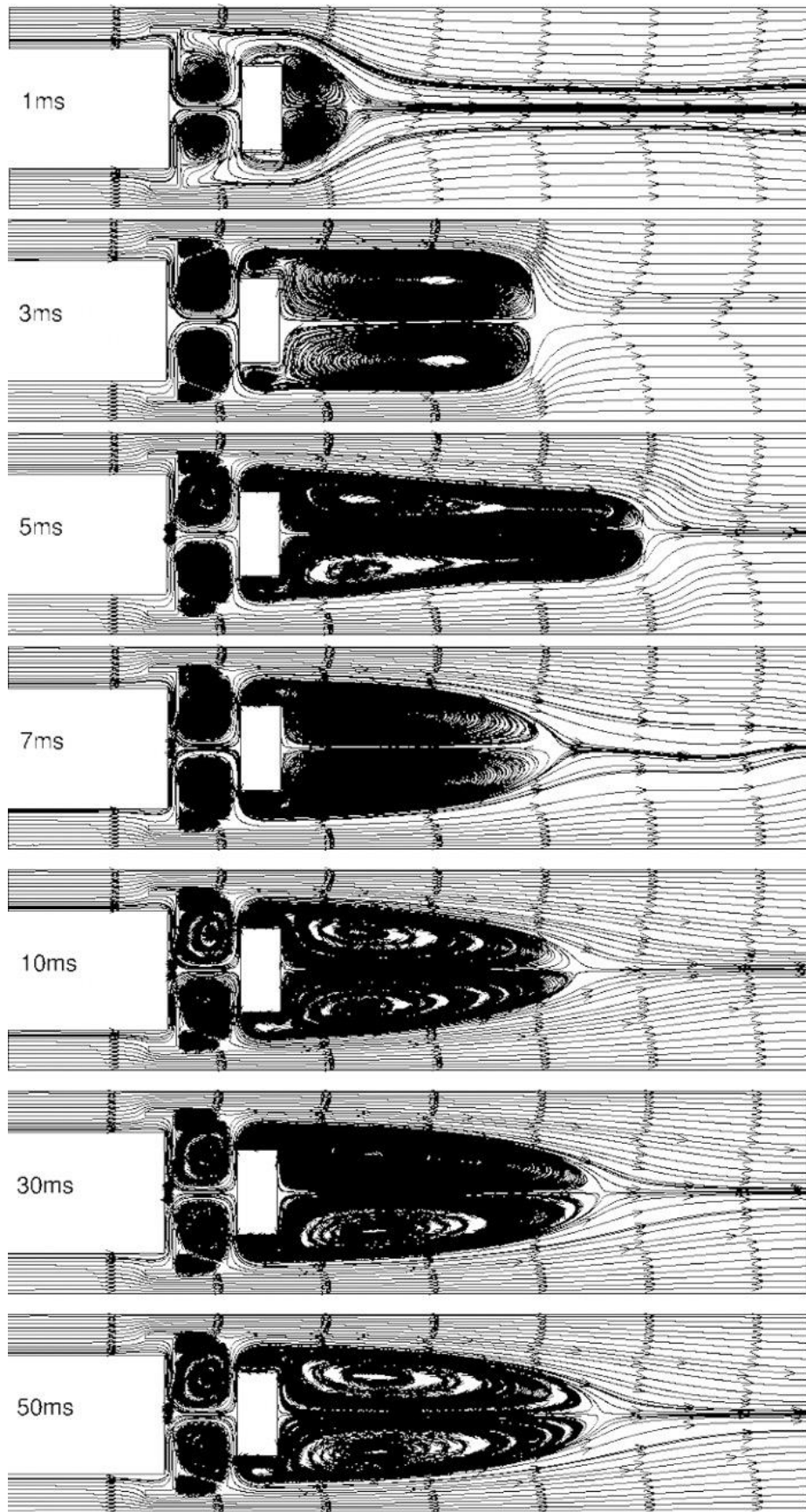


Fig. 9. Non-reacting flow field in the original combustor.

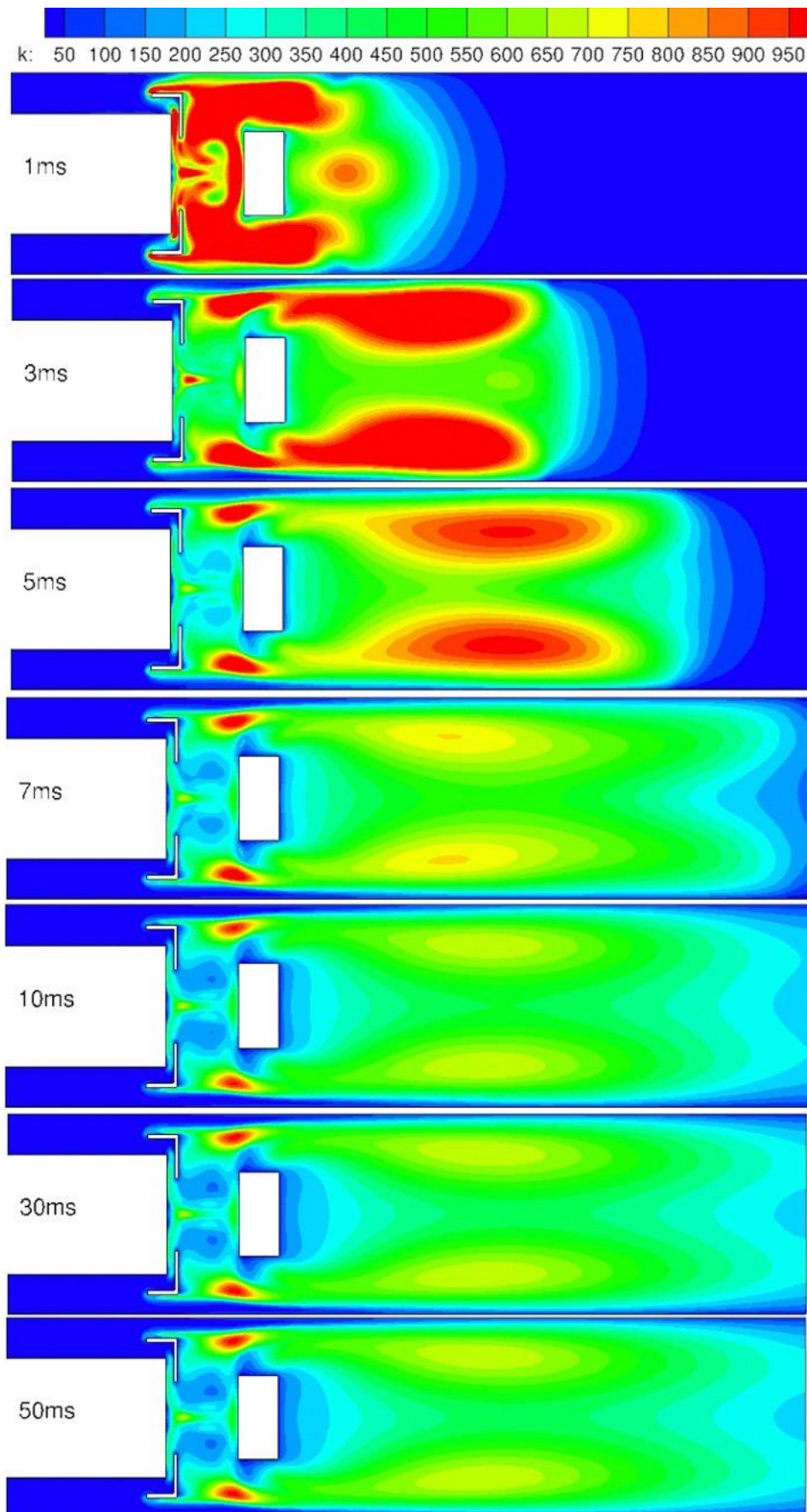


Fig. 10. Development of turbulent kinetic energy.

Fig. 11 presents the instantaneous flow field of the modified model under nonreacting case. The overall sizes used in this case are $l/L=0.5$, $C/H=0.1$, $\theta = 45^\circ$. Similar to the original case, the vortices are not fully developed at the beginning and small vortex structures are not present in the upper and lower part of the rear blunt body and after the cross-section. The most obvious difference between original and modified models is that at 3ms and 5ms, the main vortex is not growing that long due to the presence of the convergent cross-section. A couple of vortices are formed after the variable cross-section and they continue growing after the rest of vortices are fully developed. Specifically, from 7ms to 50ms, vortices inside the cavity and behind the rear blunt body are almost stable but the couple of small vortices near the wall are still growing. Compared with the original model, modified one reaches steady state in a shorter time. At about 5ms, main structure of vortex has been almost the same as 50ms. In addition, the mainstream has little effect on the streamline of the big vortex after the rear blunt body as well as vortices inside the cavity. The structure of the big vortex is compressed due to the design of reduced chamber cross-section.

Fig. 12 shows the development of turbulence energy in the modified model. Taking into account that the level of turbulent kinetic energy of original and modified model is different and the latter is higher, up to 1100, but the former is only up to 950. Similarly, higher turbulent kinetic energy appears in the front section of the chamber at the beginning of the simulation, which can also be stated that higher turbulent kinetic energy is distributed around the rear blunt body. From 1ms to 3ms, the circular core of the higher turbulent kinetic energy moves to the middle of the chamber and at the same time, the higher turbulent kinetic energy inside the cavity starts disappearing, but doesn't reach a very low value at this time instant. Compared with 3ms, at 5ms, turbulent kinetic energy inside the cavity continues decreasing and higher turbulent kinetic energy goes towards the outlet along the mainstream. Besides, the concentrated higher turbulent kinetic energy distribution is reduced and it spreads in the whole chamber. With the time increases, the higher turbulent kinetic energy inside the cavity still becomes lower. Another difference between original model and modified one is that lower turbulent kinetic energy takes a larger area near the outlet section. The collected higher turbulent kinetic energy lump separates into two parts and symmetric with each other. The tail of the turbulent kinetic energy grows from 1ms to 7ms and reaches maximum. But it starts reducing after 7ms and tends to be constant after 10ms. Also, turbulent kinetic energy is small near cavity afterwall.

In summary, the modified model can achieve more stable combustion compared with the original one due to its vortices become stable more quickly.

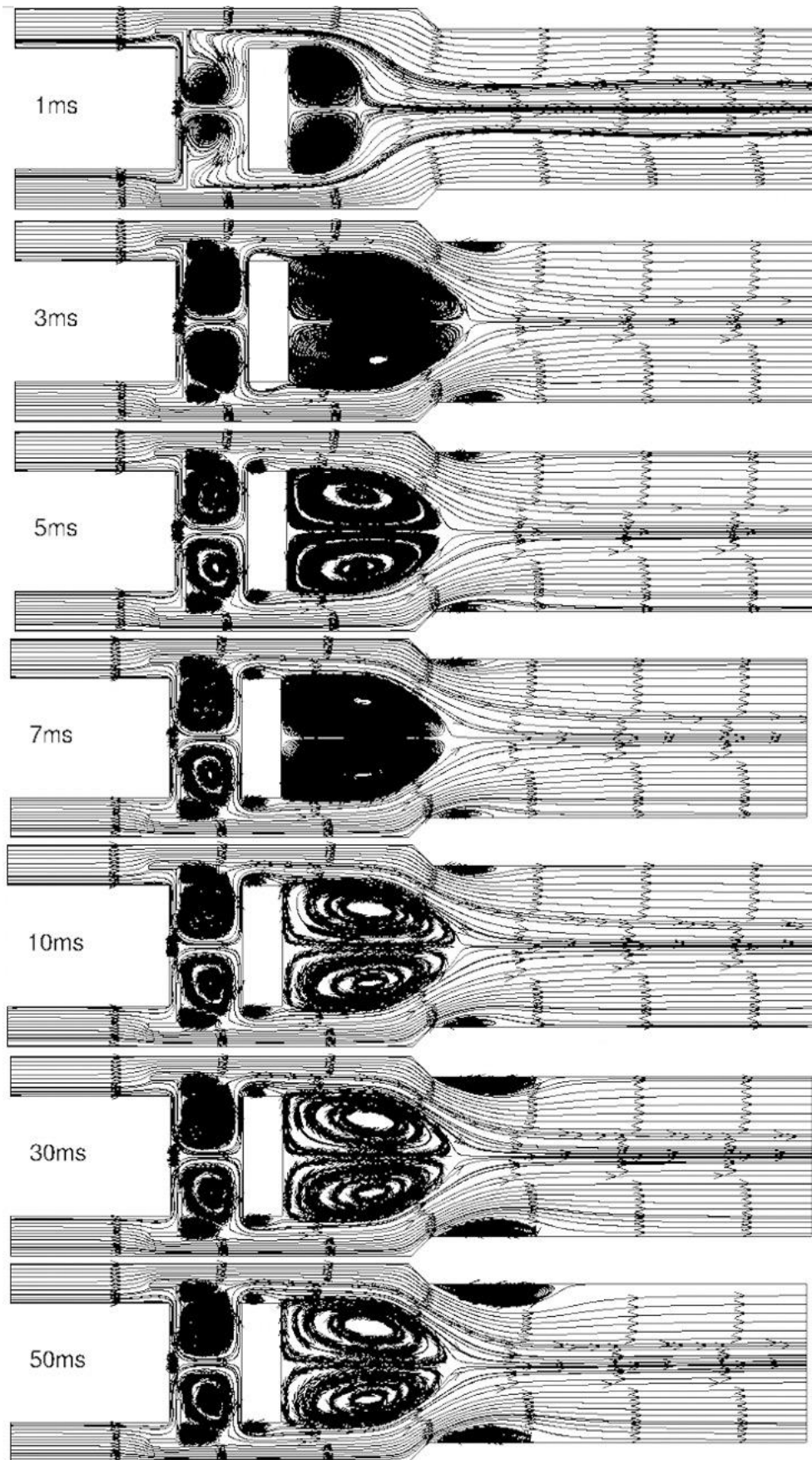


Fig. 11. Instantaneous flow field of the modified model under nonreaction.

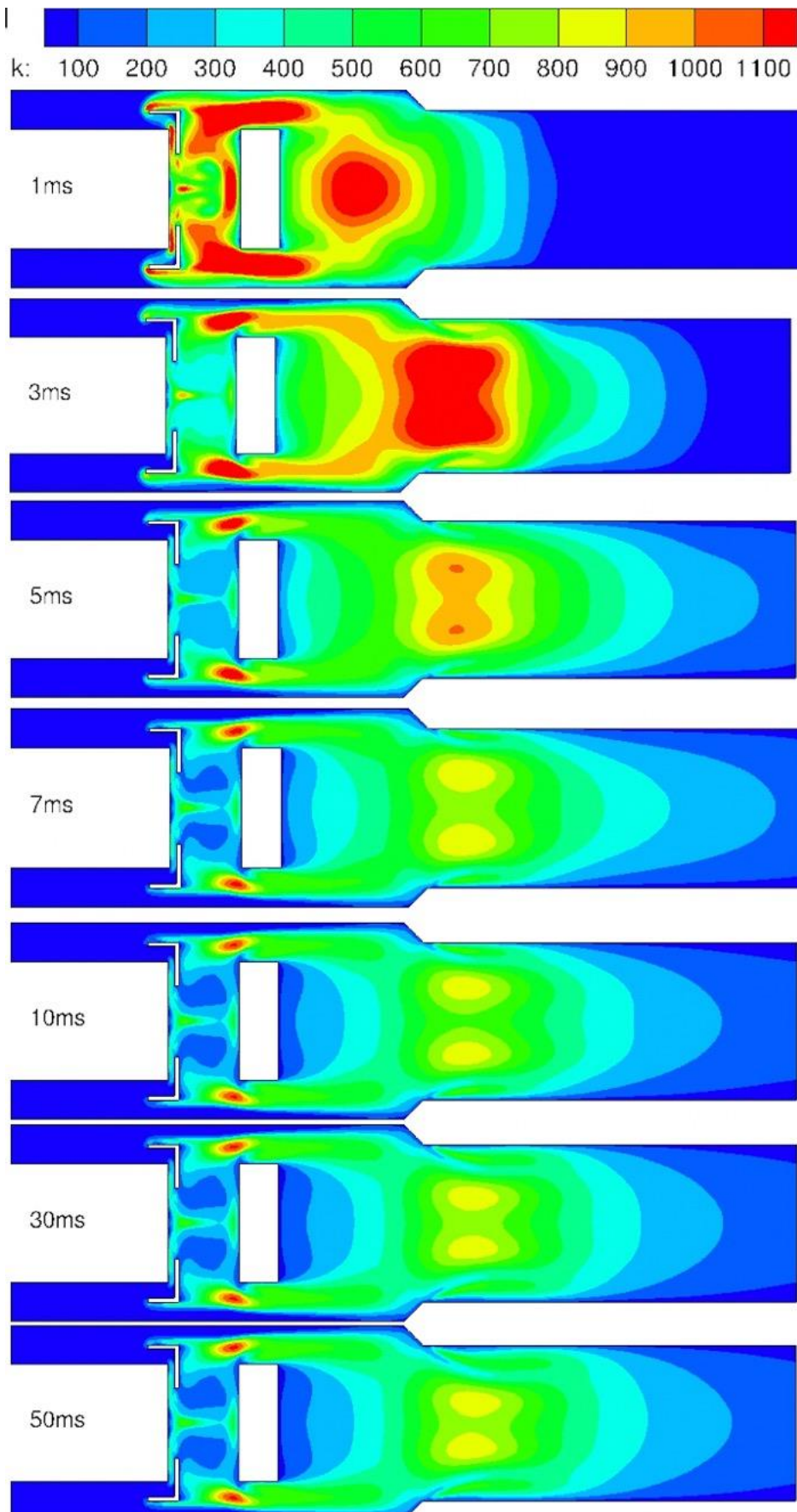


Fig. 12. Development of turbulence energy of the modified model under nonreaction.

As shown in Fig. 13, combustion flow field is plotted. Due to in this case we set the time instant for ignition is 5ms, so from 1ms to 5ms, the flow field is the same with the nonreacting flow. Starting from 6ms, double-vortex structure inside the cavity and near rear blunt body afterwall disappear and we can see clearly the sites for initial ignition both inside the cavity and near afterwall of the rear blunt body. At 6ms, the previously formed vortices completely disappear and in the subsequent time instant, they begin to grow. As we can see, the vortex inside the cavity is growing more quickly than that near the afterwall of the rear blunt body. At 7ms, a couple of small vortices initiate in the upper and lower part of the afterwall of the rear blunt body, then further develop. At 10ms, the couple of large vortices are not affected by the mainstream even near the reduced cross-section, so the vortex looks more fully developed but on the contrary, the mainstream is little affected by the main vortices. From 7ms to 10ms, double-vortex structure inside the cavity is initially formed and then disappear. At 20ms, double-vortex inside the cavity is formed again and the area of the main vortices is compressed due to the effects of the decreased cross-section. From 20ms to 50ms, internal flow field is almost achieving steady state and 6 couple of vortex can be visualized. Three couples of them are located in the cavity and one is located in the upper and lower part of the rear blunt body and another one is near the afterwall of the rear blunt body. The last one is located near the wall and just after the variable cross-section. Compared with cold situation, vortices near the afterwall and near the wall in the hot case are relatively smaller, especially for the vortices near the wall.

Fig. 14 presents turbulent kinetic energy distribution of the reacting flow. We can easily find that due to the reaction, turbulent kinetic energy is much higher than nonreacting case and up to 1,800. The difference is that at 10ms, which is the time instant that vortices regenerate, the turbulent kinetic energy is forced to move to the center of the chamber and lower turbulent kinetic energy occupies a higher portion of area. In the cold case, a couple of higher turbulent kinetic energy lumps appear in the center of the chamber but in hot case, it is not separated. This core is located in the tail of the main vortices, which means higher blending in this site. We can also see the mainstream with low turbulent kinetic energy is not affected by the vortices and vortex is not affected by the main streamline, which indicates that the combustion in our model is stable.

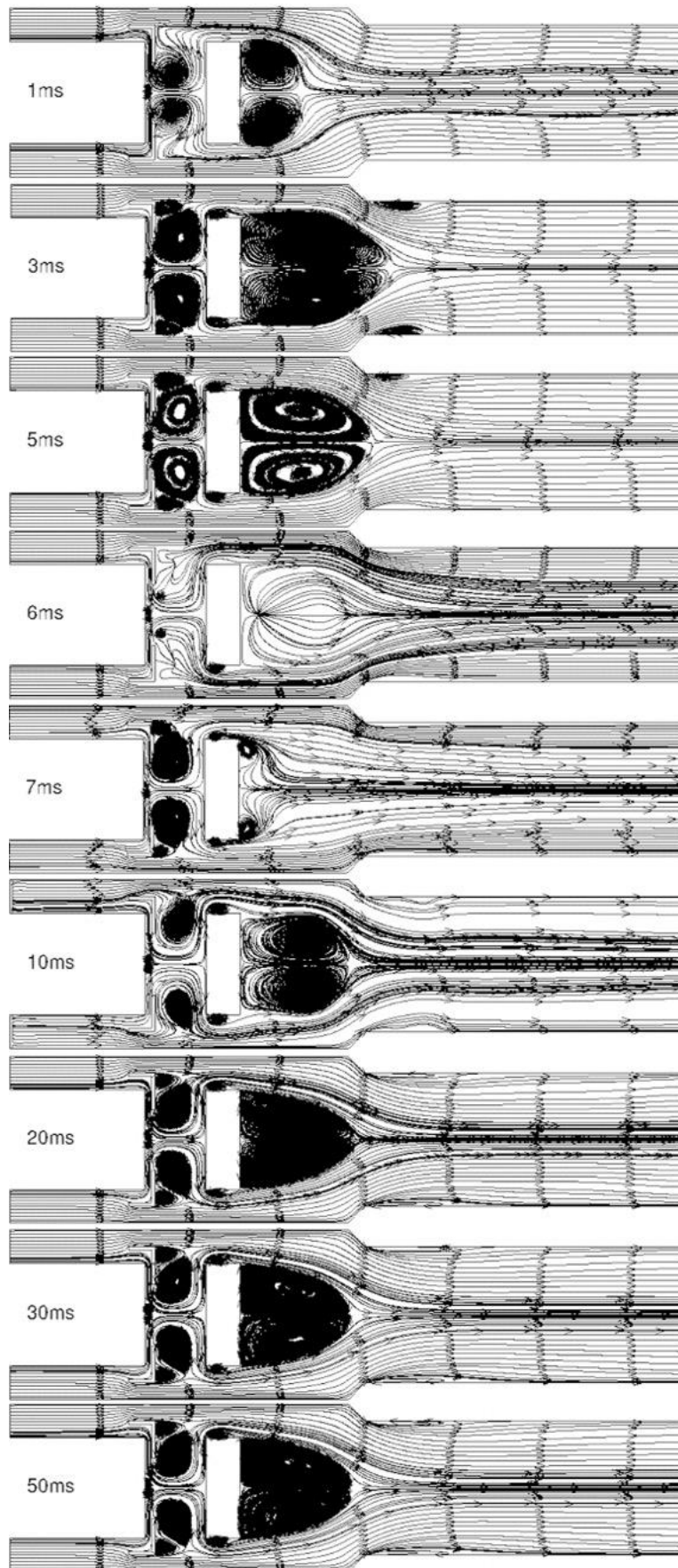


Fig. 13. Instantaneous flow field of the modified model under reaction.

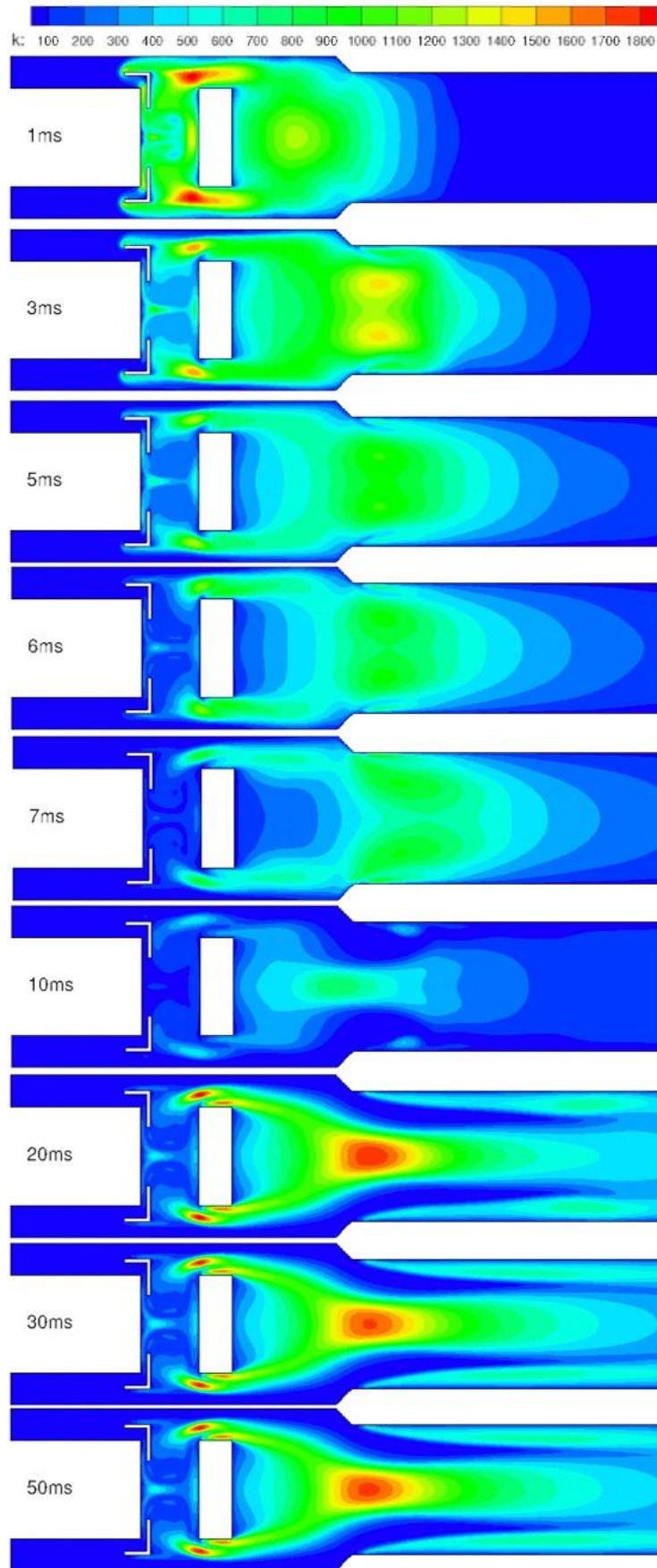


Fig. 14. Development of turbulence energy of the modified model under reaction.

Temperature changes with time can be shown in Fig. 15. As aforementioned, we ignite at time instant 5ms, so the temperature before 6ms is just the initial condition. Starting from 6ms, previously setted high temperature points work as ignition sources. At 7ms, higher temperature mainly appears in the positions where vortices are present such as cavity and near the afterwall of the rear blunt body. From 7ms to 10ms, higher temperature spreads in the whole chamber. Then, from 10ms to 30 ms, the structure of the higher temperature zone is almost the same but the temperature inside the cavity is slightly decreased.

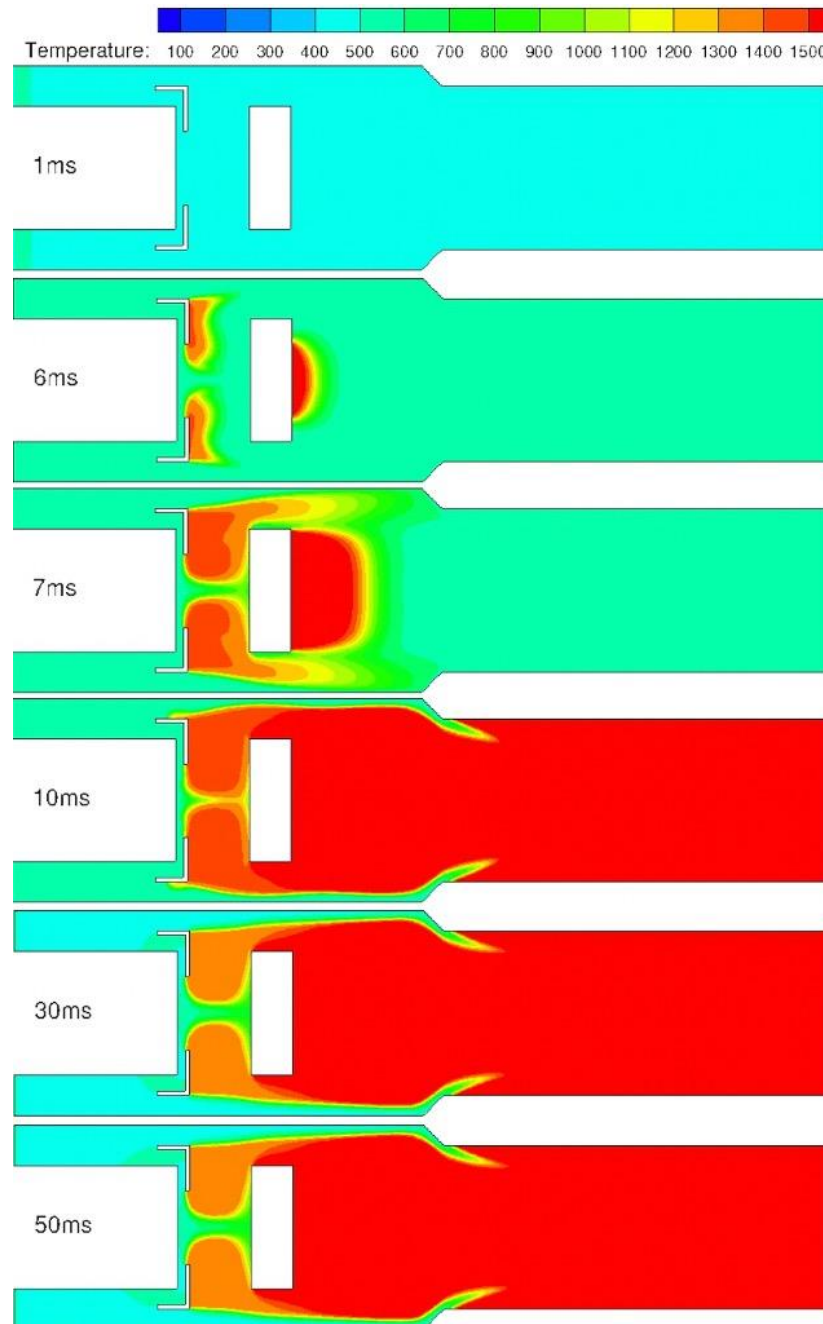


Fig. 15. Temperature changes with time.

In this chapter, we numerically carried out the comparison between the original model and model both in cold and hot cases. Transient development of the vortices, flow field, turbulence kinetic energy and temperature distribution are analyzed. The results shows that the modified model is able to achieve more stable combustion and more uniform temperature distribution. The latter can reduce the thermal stress.

4. Studies of geometrical parameters of the variable cross-section.

The size of the variable cross-section has obvious influence on the performance of the modified combustor, so it is necessary to study the size of the proposed variable cross-section. In the following section, three groups of parameters will be discussed. They are listed in Table.1.

Table 1. Parameters that will be analysed.

Variables	Values				
$C/H [-]$	0.03	0.06	0.09	0.12	-
$l/L [-]$	0.25	0.3	0.4	0.5	0.6
$\theta [^\circ]$	0	15	30	45	60

4.1 Influence of the value of C/H on the performance.

In this case, we study the changes of the flow field and temperature field with time under the same geometric size. Fig. 16 shows the instantaneous development of internal field when the value of C/H is 0.03. Similarly, we set ignition time at time instant 5ms, so from the plot at 6ms, the flow field is initialized. From 7ms to 10ms, vortices start growing and the growth of main vortices even have effect on the flow trajectory. At the same time, double-vortex structure diminishes and only one couple of big vortex are left in the cavity. With the time increases, previously extinguished double-vortex structure formed again and at time instant 30ms, the flow field is not perfectly symmetric and small oscillation is existing. From 50ms, everything does not vary with time. Due to the small size of the undercut, the influence is slight, but the field reaches stable slowly compared with other size of undercut.

Temperature changes with time are illustrated in Fig. 17. Same as other cases, ignition time is set at 5ms, therefore flame mainly develops from 7ms. At 12ms, we can easily find that the mainstream is affected and changes its direction of flow, and this behaviour will increase the mixing of burnt and unburnt gases improving combustion efficiency. The shortcoming is total pressure loss will increase. So the size of the undercut should not be very large. Not as detailed

as the flow field, it's hard to find the asymmetry details inside the burnt area because their temperature is almost the same, and we find that from 20ms, the temperature field is almost steady. At 12ms, the tails of the lower temperature zone are relatively wider but shorter compared with the case at 20 and 50ms and these tails are almost along the wall.

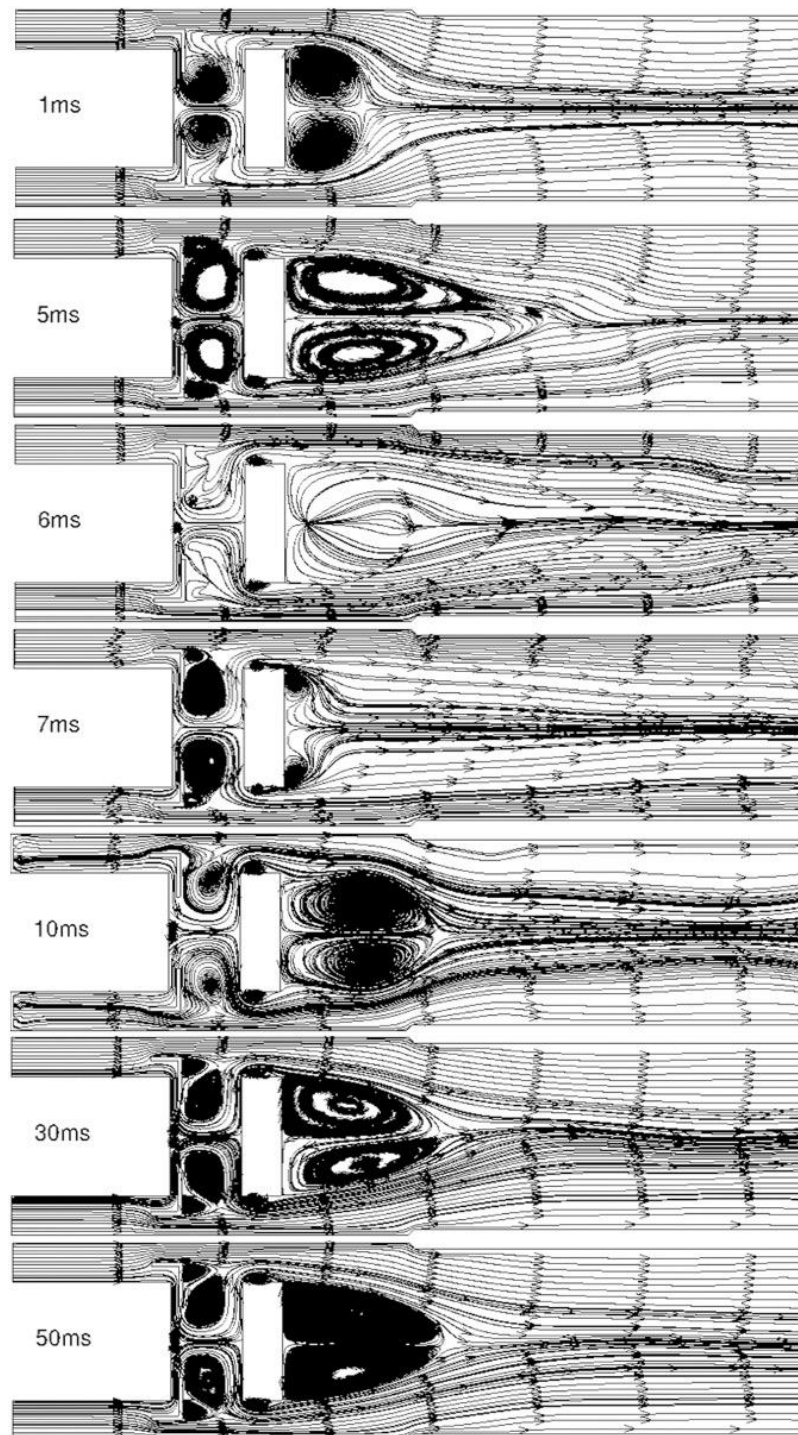


Fig. 16. Instantaneous development of flow field when the value of C/H is 0.03.

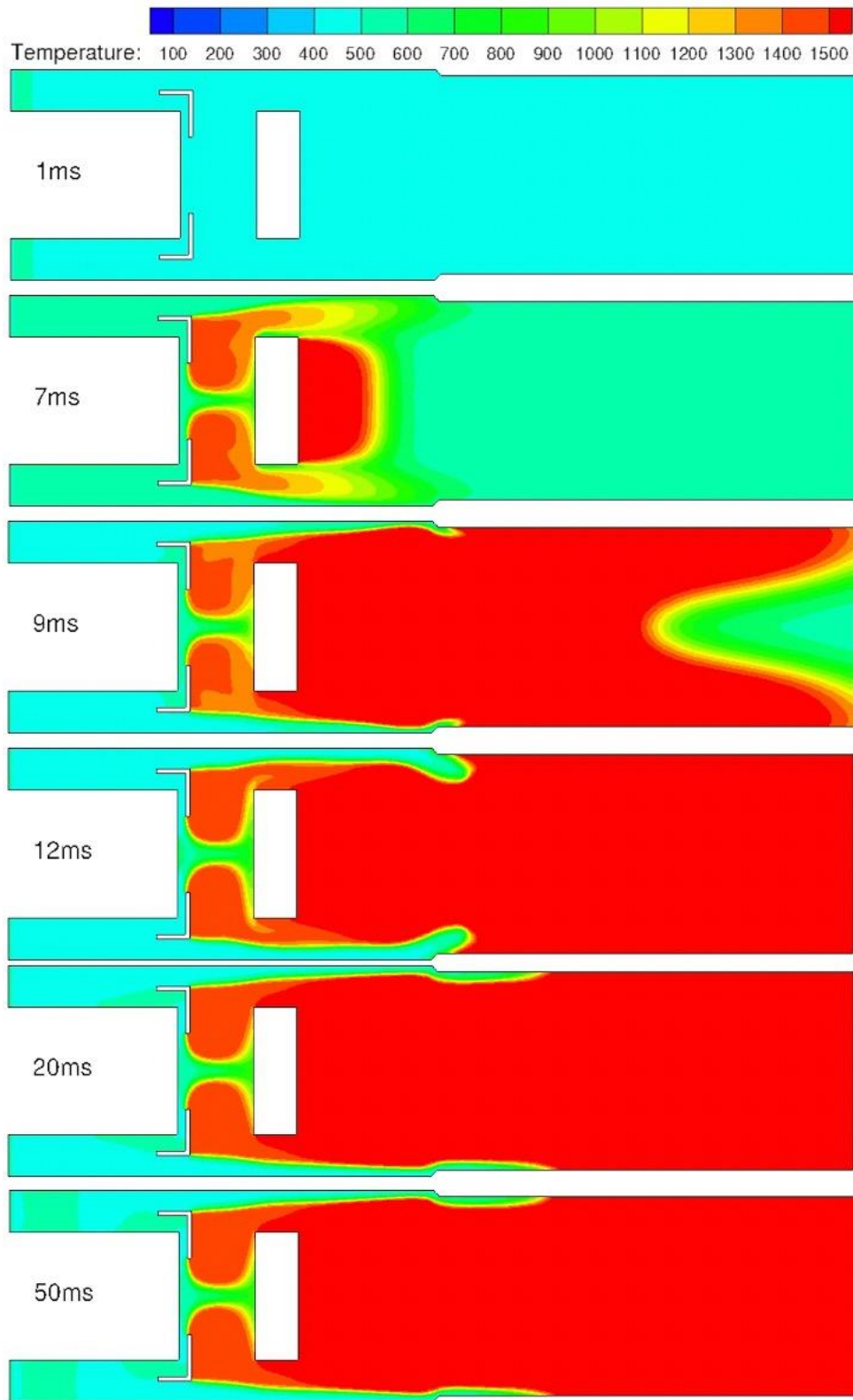


Fig. 17. Instantaneous development of temperature field when the value of C/H is 0.03.

Fig. 18 and Fig. 19 give information about the flow and temperature field when the magnitude of C/H is 0.06. Compared with the previous one, the difference is that at 10ms, a couple of small vortices are generated near the wall. The reason is that in the previous case, the aforementioned couple of small vortices are not present is that the size is too small to generate such kind of effect. This couple of vortices are stretched to be very thin and the main vortices near the afterwall of the rear blunt body is further compressed. From Fig. 19, it is found that unlike the previous case, the tails of the lower temperature zone have a certain angle with the wall.

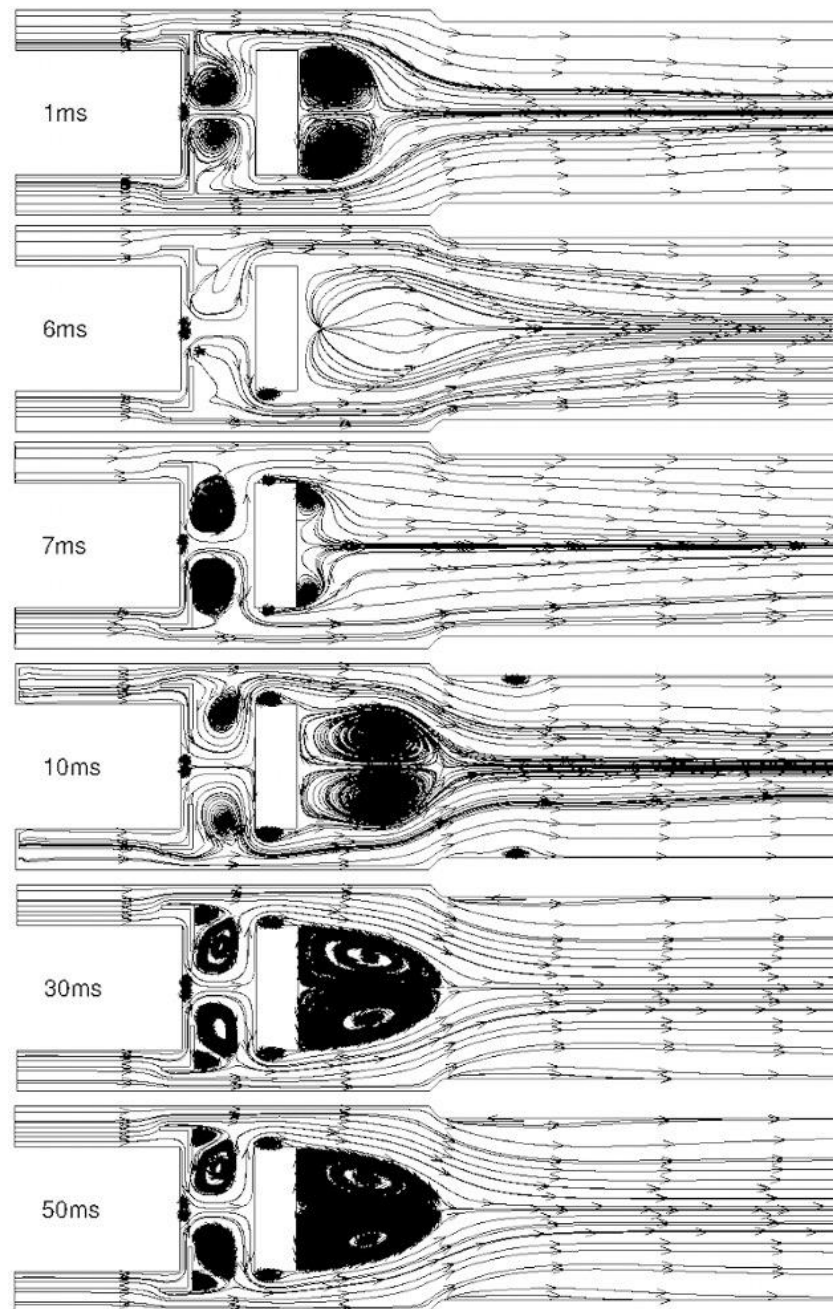


Fig. 18. Instantaneous development of flow field when the value of C/H is 0.06.

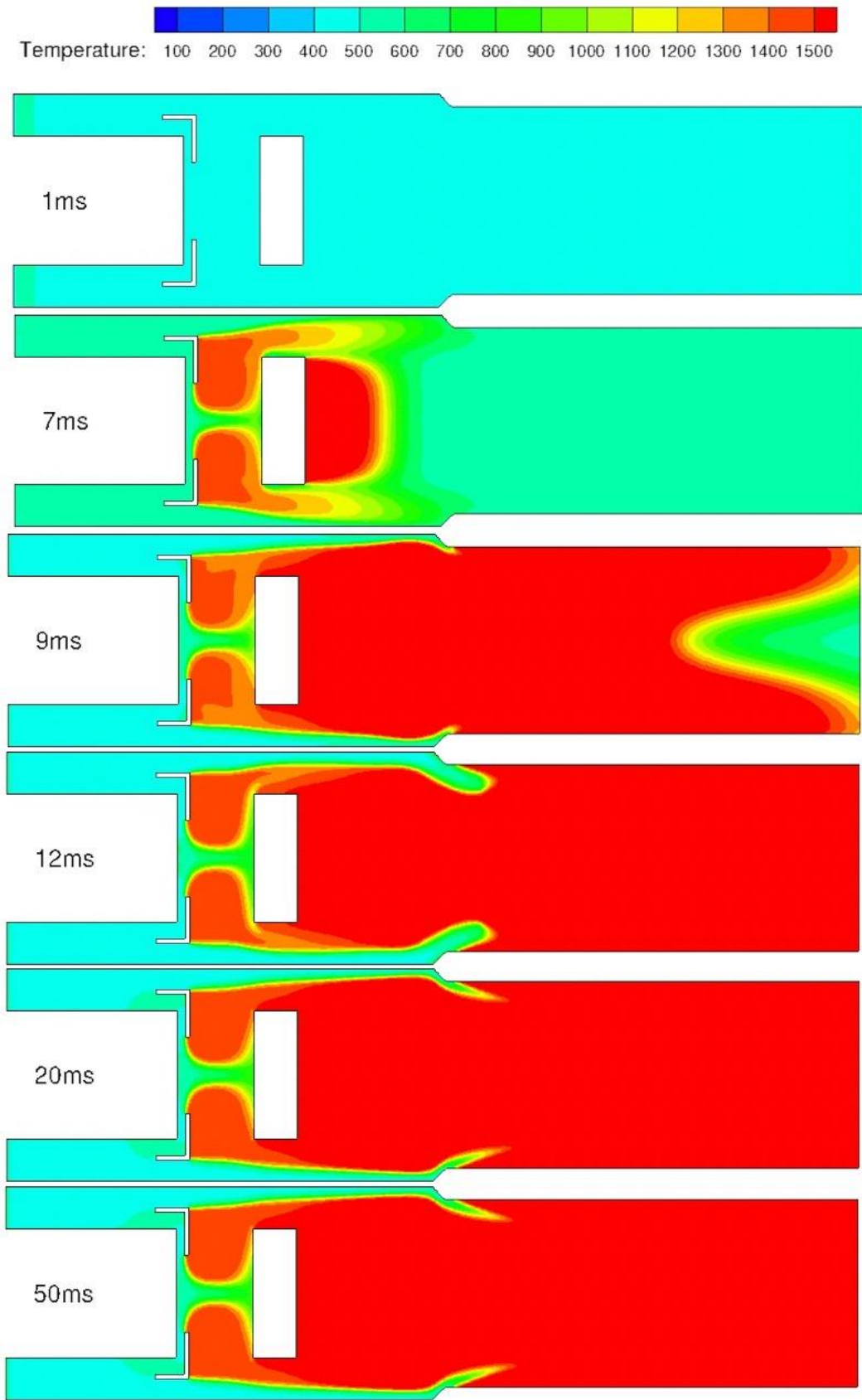


Fig. 19. Instantaneous development of temperature field when the value of C/H is 0.06.

Fig. 20 and Fig. 21 depict the situations when the value of C/H is 0.09 and 0.12, respectively. They show little difference from previously discussed cases but at 10ms, when C/H is 0.12, the couple of small vortices are not able to form. In addition, With the size of the undercut increasing, the area of the main vortices near the afterwall of the rear blunt body is reduced due to the effect of the reduction of the cross-section of the flow channel. Another point that is worth mentioning is that when C/H is 0.12, the temperature inside the cavity is slightly lower than other cases. Actually, starting from the value of C/H is 0.09, the temperature inside the cavity is decreasing.

In summary, the size of the undercut has small effect on the performance of the combustor but it should not be too large to avoid high total pressure loss.

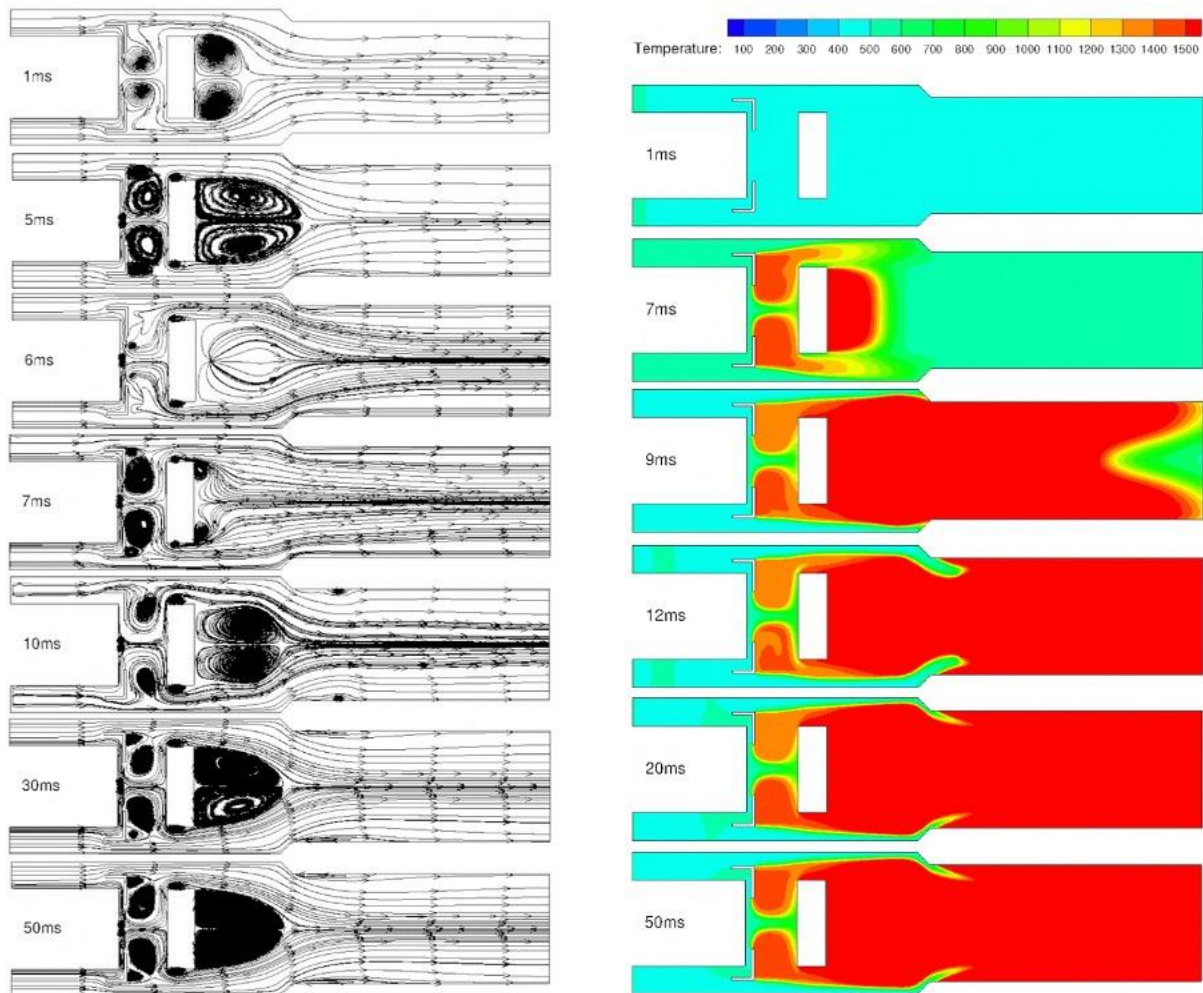


Fig. 20. Development of flow and teperature field when the value of C/H is 0.09.

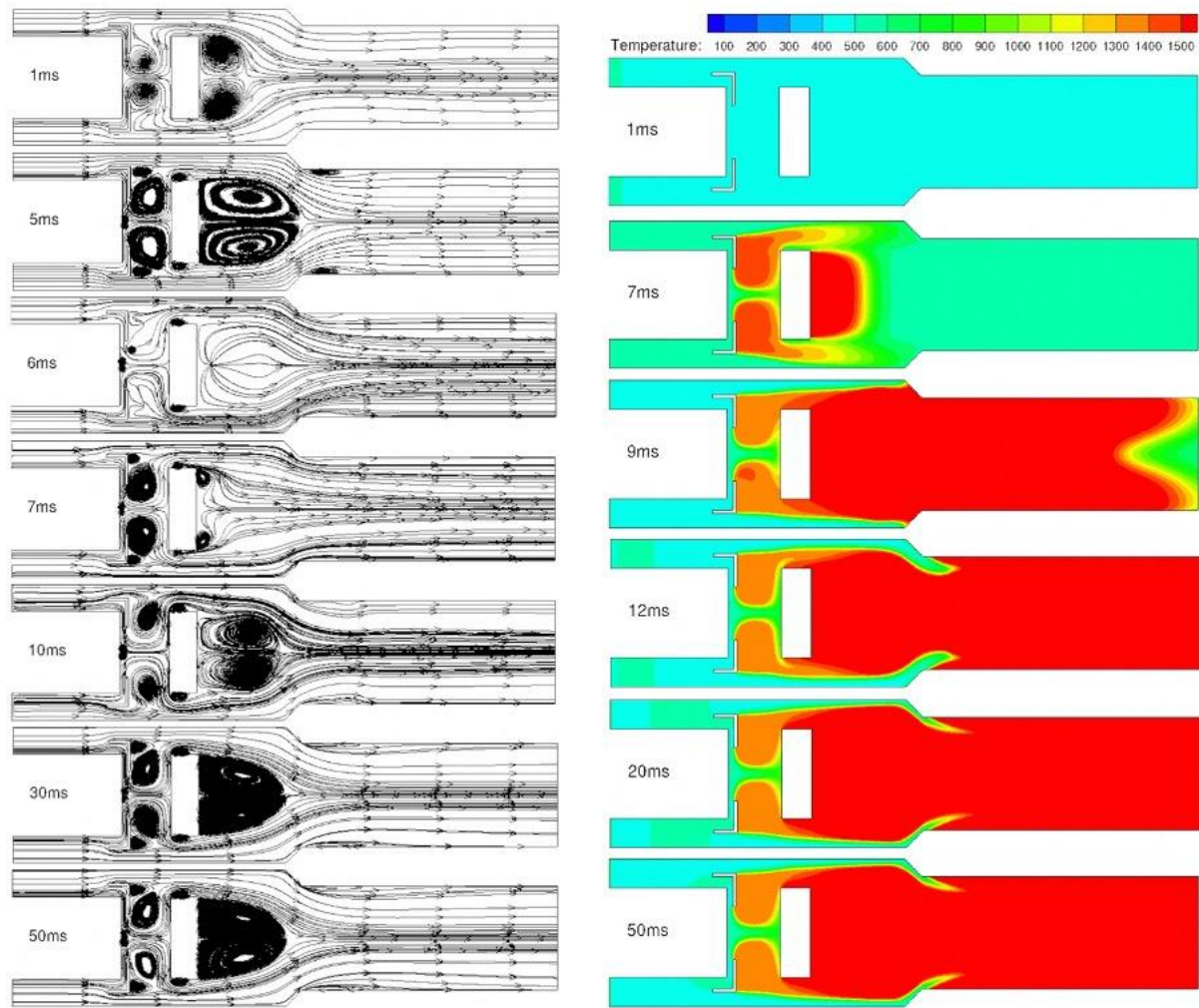


Fig. 21. Development of flow and temperature field when the value of C/H is 0.12.

4.2 Influence of the value of l/L on the performance.

In this situation, different from the previous method of analysis, under different geometric dimensions, the flow field and temperature field at the same time instant will be compared to study another aspect of the effect of the geometry. Due to the fact that the ignition time is set at 5ms, so Fig. 22,23 and 24 are nonreacting flow cases.

Fig. 22 shows at 1ms, comparison between different groups of l/L values are made. We can clearly see that when the reduction of the area of the channel is near the guide vanes such as when l/L is 0.25, the vortices behind the rear blunt body are less affected but have more effects on the vortices inside the cavity. It is easily found that when the magnitude of l/L is increasing, the vortices inside the cavity become larger but the size of vortices behind rear blunt body is compressed at the beginning. What is the same is that there is no case being able to generate double-vortex structure at the beginning.

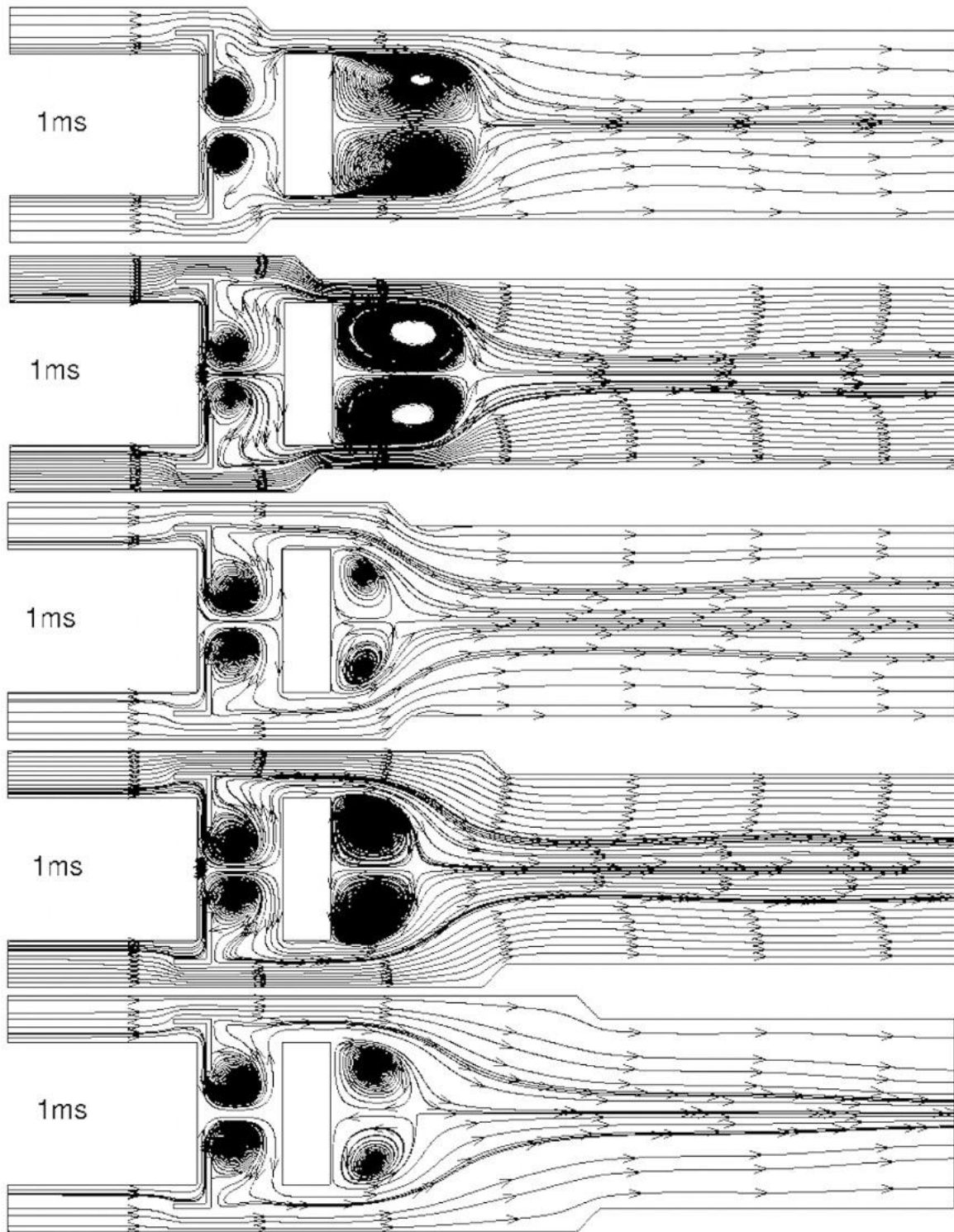


Fig. 22. Comparison between different groups of l/L at 1ms.

Fig. 23 presents flow fields at 3ms for different values of l/L . When the value of l/L is smaller than 0.4, the couple of small vortices are not able to be generated. From 1ms to 3ms, each couple of vortices continue growing and double-vortex structure is formed starting from 3ms. The length of the main vortices become very large when the value of l/L is small and the length is in a intermediate range when the value of l/L is in a proper range. Too large size of

recirculation zone will lead to more pressure loss and the flow field tends to be unstable. But too small recirculation zone is not conducive to stabilize the flame and ignite the fuels. Therefore the site of the variable cross-section should be chosen carefully. In addition, a couple of small vortices in the upper and lower part of the rear blunt body, which can serve as ignition sources, can only be generated when the value of l/L is higher than 0.4.

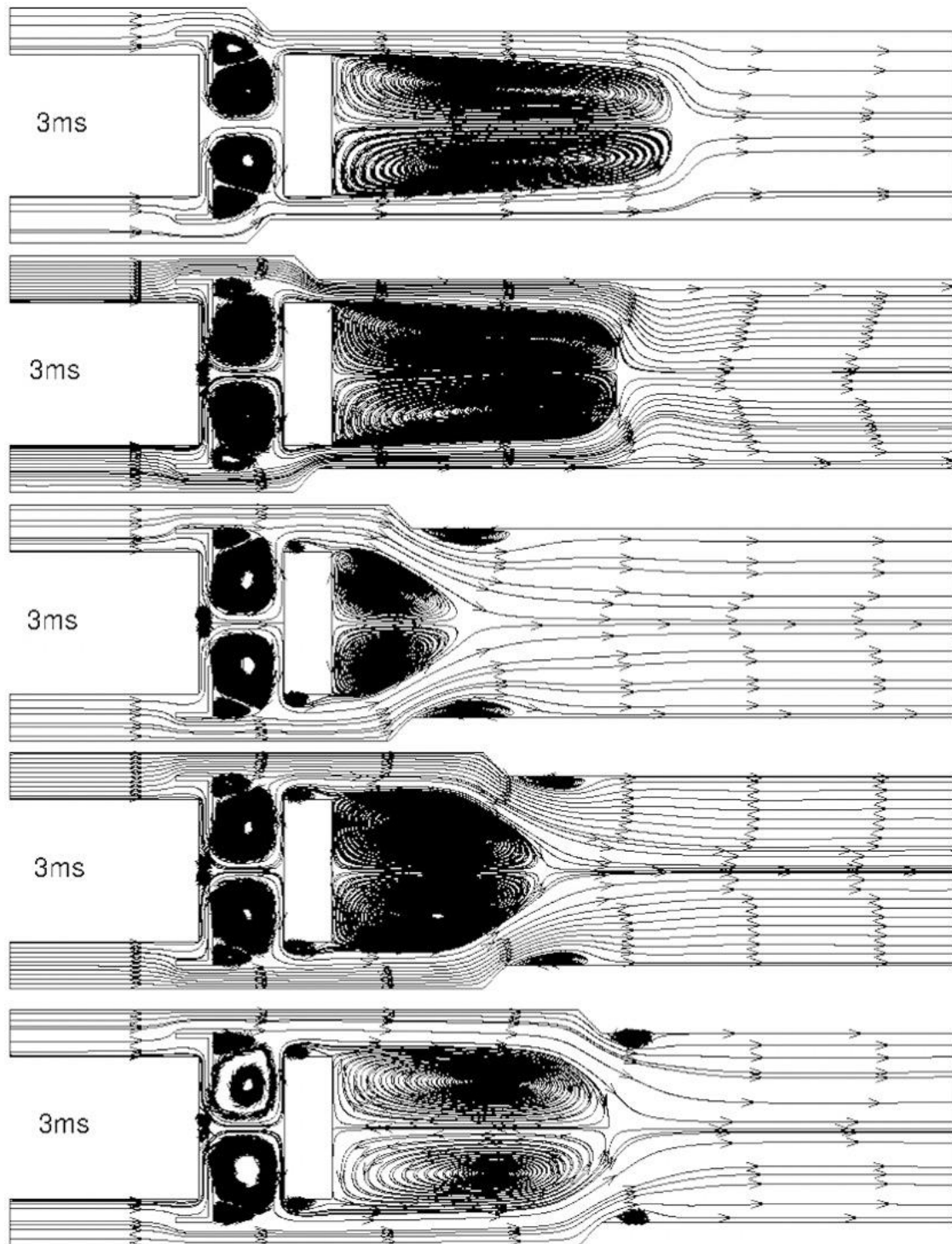


Fig. 23. Comparison between different groups of l/L at 3ms.

Fig. 24 shows what happens under different positions of the bevel, which is the distance from inlet to the position in which the reduction of the area of the channel is designed. When the ratio between l and L is lower than 0.4, the instant field at 5ms is not completely symmetric, which means the flow field is not stable. Compared with 3ms, the main vortices are further compressed but vortices inside the cavity almost remain the same.

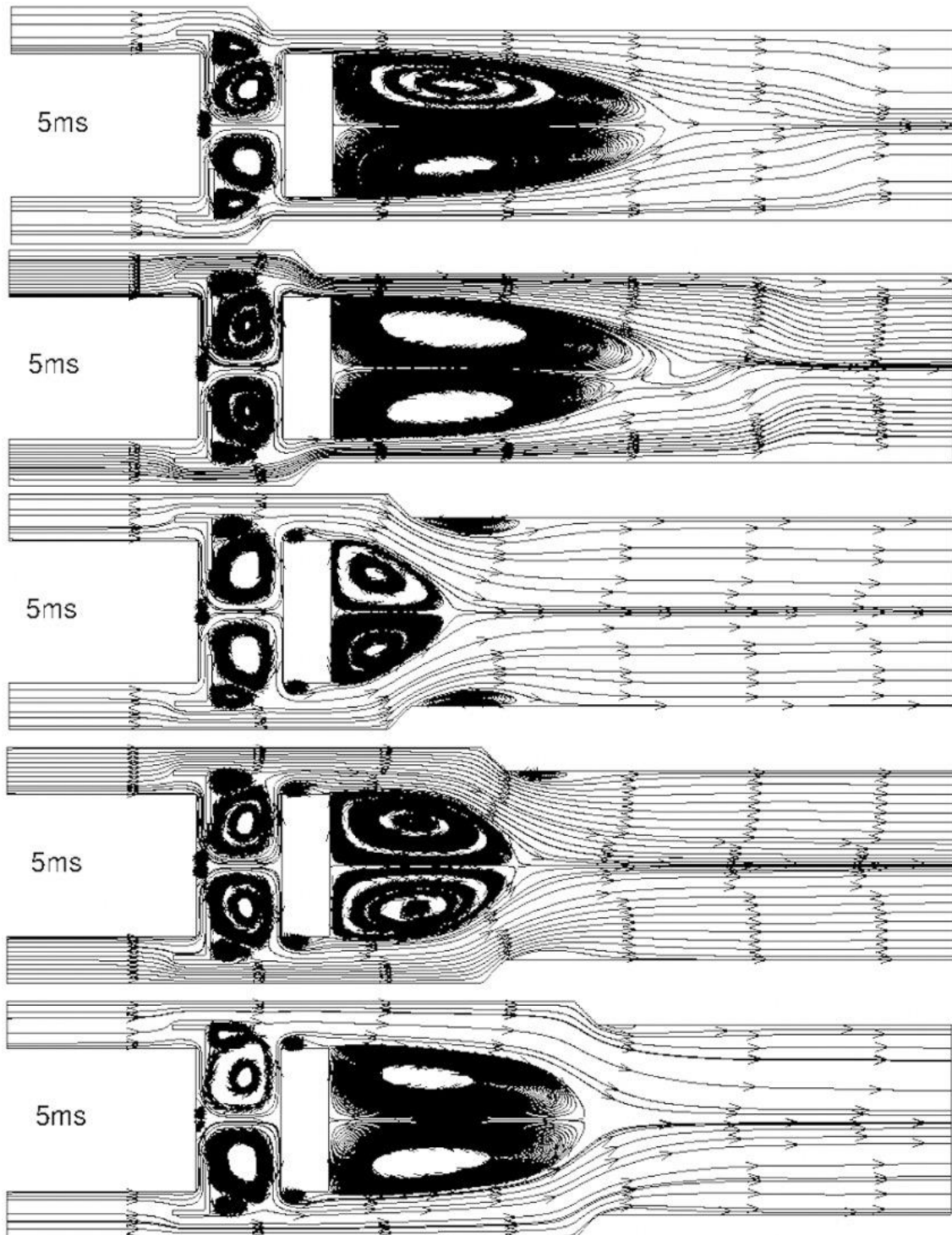


Fig. 24. Comparison between different groups of l/L at 5ms.

As is shown in Fig. 25, the flow fields at 6ms, which is the beginning of the ignition, are illustrated. There are no vortices being generated when l/L is equal to 0.4 and 0.5 at this time instant. A couple of relatively bigger vortices are formed after the guide vanes when the value of l/L is 0.25. The reason is that the inclination forces the formation of the vortices and the residence time of the gases will be increased in this area.

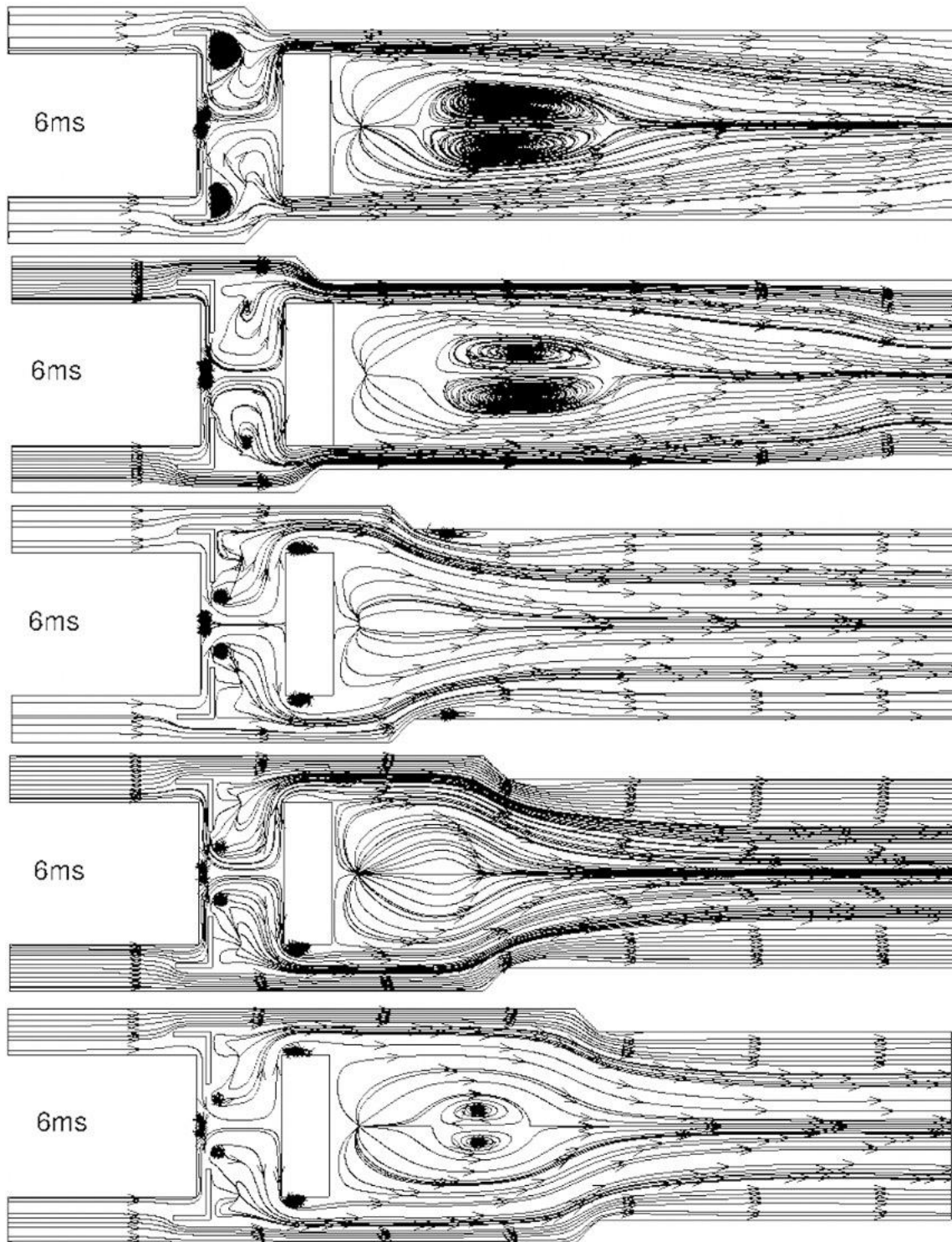


Fig. 25. Comparison between different groups of l/L at 6ms.

Fig. 26 reveals 4ms after the ignition, we can find that main vortices have been initially regenerated and vortices inside the cavity is growing but the case when l/L is 0.4 is an exception. The speed of the growth of the vortices of the model in which l/L is 0.5 is the fastest and when l/L is 0.4, from 6ms to 10ms, the vortices inside the cavity disappear. At 10ms in the case of l/L is 0.4, the main vortices are significantly affected by the mainstream and the compressive effect can be obviously observed.

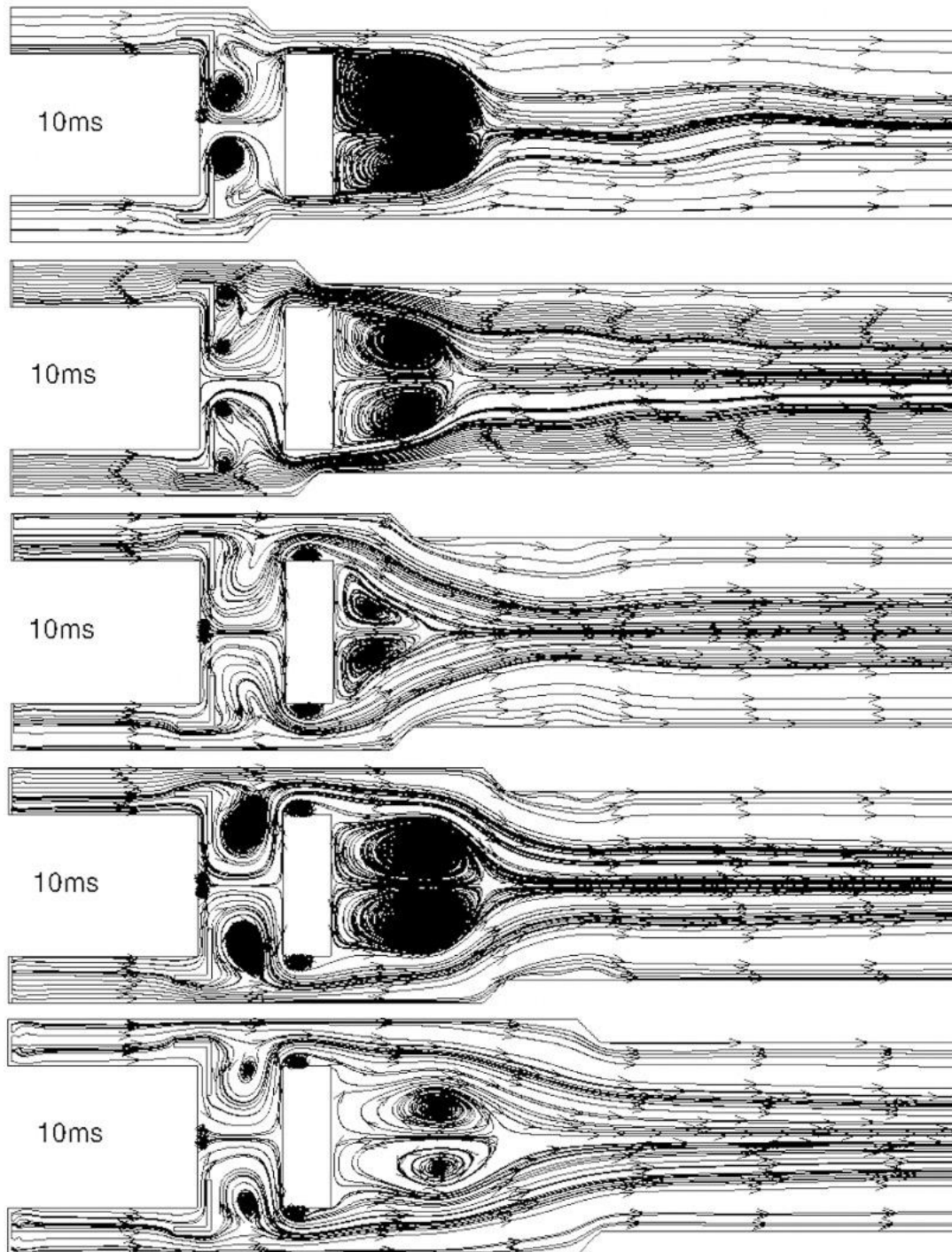


Fig. 26. Comparison between different groups of l/L at 10ms.

Fig. 27 presents the subsequent meaningful time instant which is 20ms. Asymmetry of the flow field when l/L is 0.25 and 0.3 is the most evident phenomenon among the others. The indication is that the stability in those two cases is difficult to reach, so during the design phase of the real model based on this proposal, these two cases should be considered to be avoided.

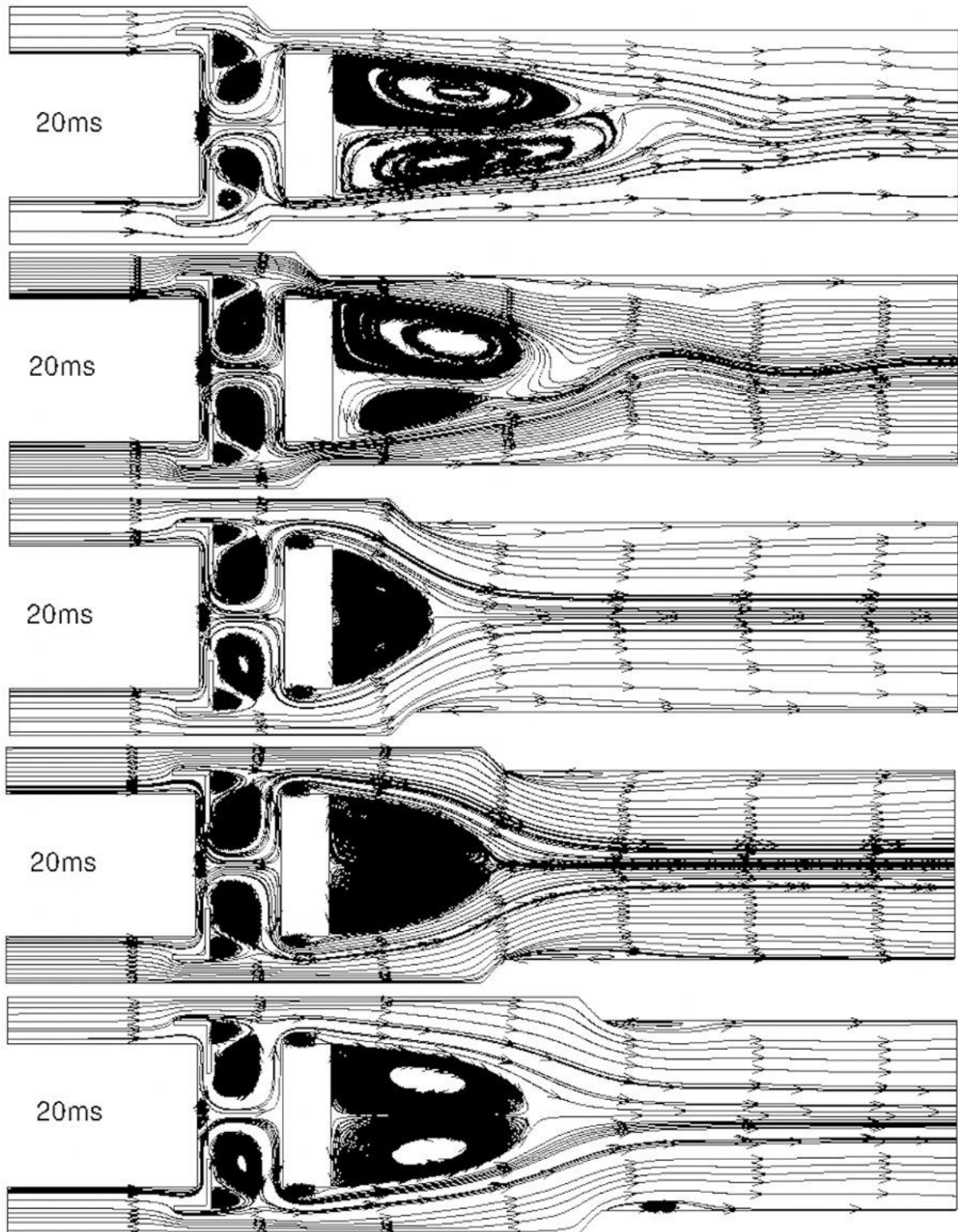


Fig. 27. Comparison between different groups of l/L at 20ms.

Then, Fig. 28 shows the instantaneous flow field at 30ms for different value of l/L . Like the previous step, asymmetric flow fields are shown in the cases of l/L is 0.25 and 0.3. For other cases, stability has been achieved and the shape and size of the characteristic vortices are fixed. When l/L is 0.4, the main vortices are too small so that they are not able to serve as effective ignition sources.

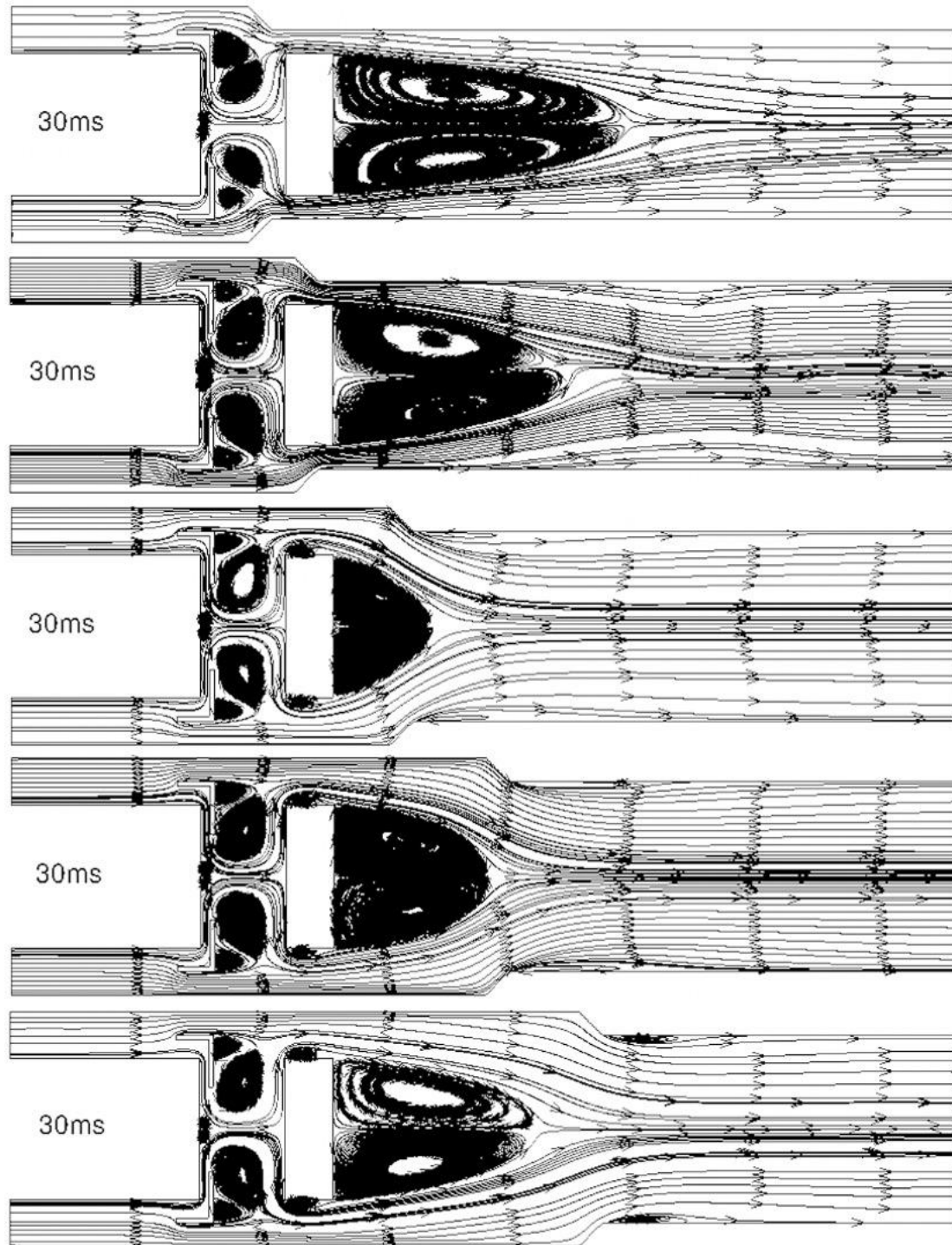


Fig. 28. Comparison between different groups of l/L at 30ms.

Finally is the time instant at 50ms shown in Fig. 29. Except the case that l/L is 0.3, the other cases have been in a stable situation. As we can see, when the value of l/L increases, the size of the vortices decreases and then increase.

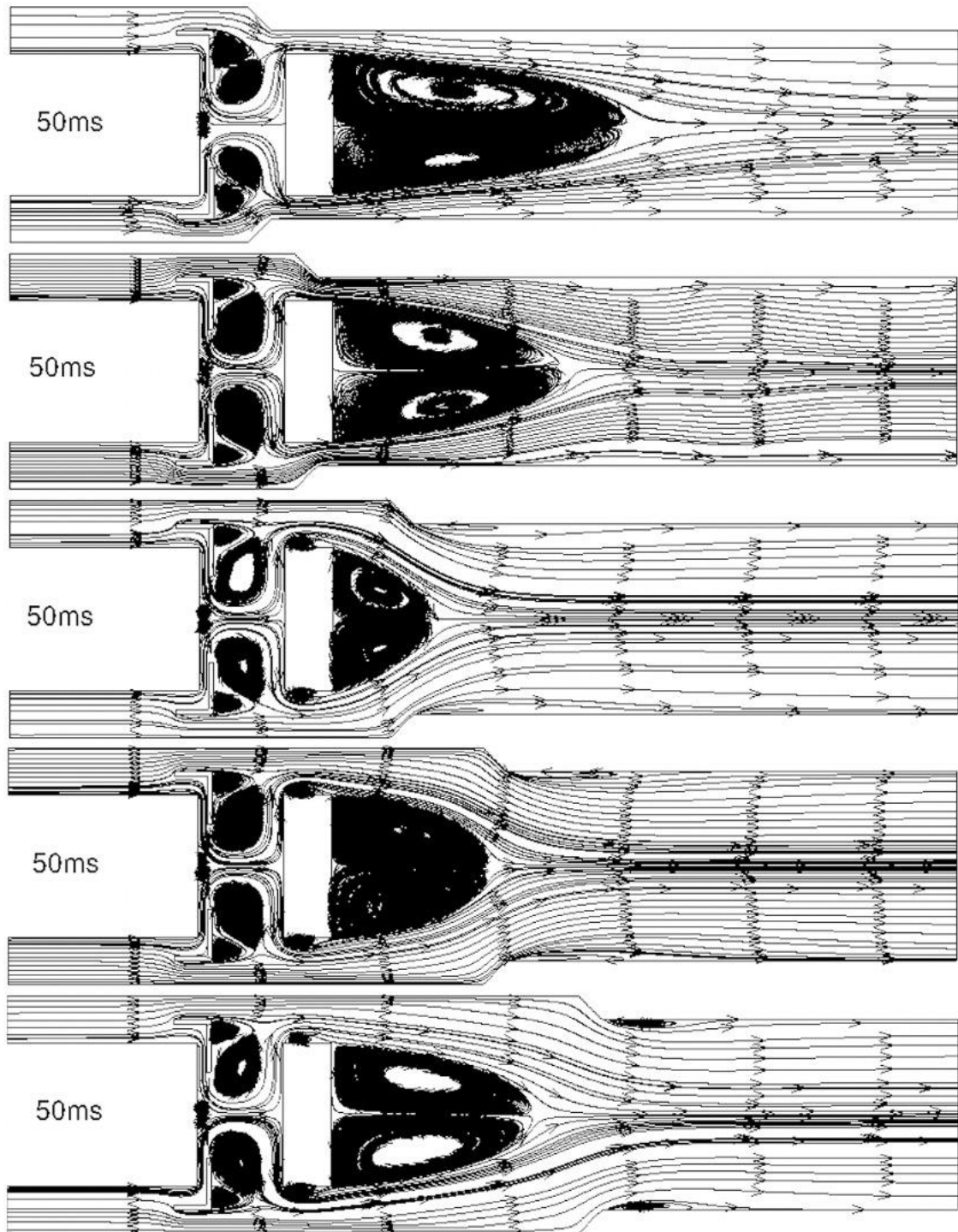


Fig. 29. Comparison between different groups of l/L at 50ms.

In summary, it is advised to avoid too large and too small size of the vortices from the view of point of stable combustion, which means that the value of l/L is about 0.5.

4.3 Influence of the value of θ on the performance.

In this case, temperature field with streamline will be studied to see the coupling and relation of two fields under different angles, which is the angle between vertical direction and inclination of the variable cross-section.

Fig. 30 demonstrates the instantaneous development of the temperature and streamline when the inclination is completely vertical. At 3ms, a couple of large vortices are formed right after the reduction position of the cross-section and they are stretched from 3ms to 6ms. The ignition process currently has no effect on these vortices but at 8ms, these vortices disappear, and at the same time, the high temperature spreads in the chamber. In the next time step, they are generated again but have two vortices in each side, main vortex is in the left and external one is in the right. From 9ms to 10ms, the external vortices experience shedding and from 11ms to 12ms until 20ms, shedding happens more than twice, which means this configuration is hard to be stable and too many times shedding will lead high pressure loss. This configuration reaches stability at about 30ms.

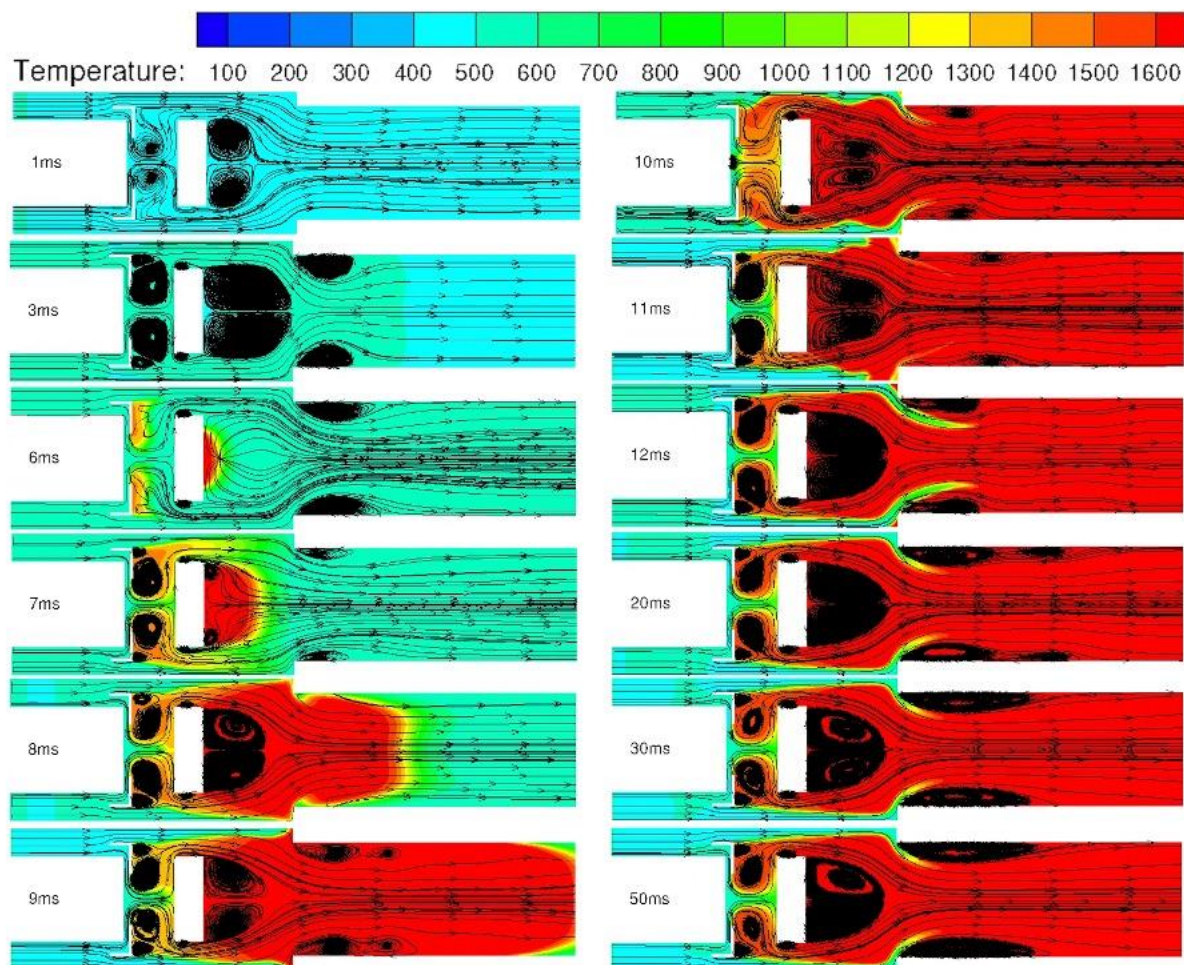


Fig. 30. Comparison between different time instant when θ is 0° .

Fig. 31 presents the situation in which the angle is 15° . Compared with the previous case, shedding of vortices only happens from 9ms to 10ms, so this case is better than the former one, and if the transition angle is too sharp such as completely vertical, pressure loss will increase significantly, which will result in the increases of the consumption of fuels. At 11ms, higher temperature zone occupies the whole cross-section before the variation. Then the mainstream with lower temperature breaks the block of the burnt zone and forms a pathway. At 12ms, the length of the tail of the pathway is long, but when it comes into high temperature zone, part of it is burnt, so the length reduces. When the shedding of vortices stops, the vortices near the wall continue growing until 20ms but the shape of the vortices inside the cavity and near the after wall of the rear blunt body are almost fixed. The stable flow and temperature field in this design has been reached at about 20ms, which is faster than the previous one. Hence this case is better than vertical one.

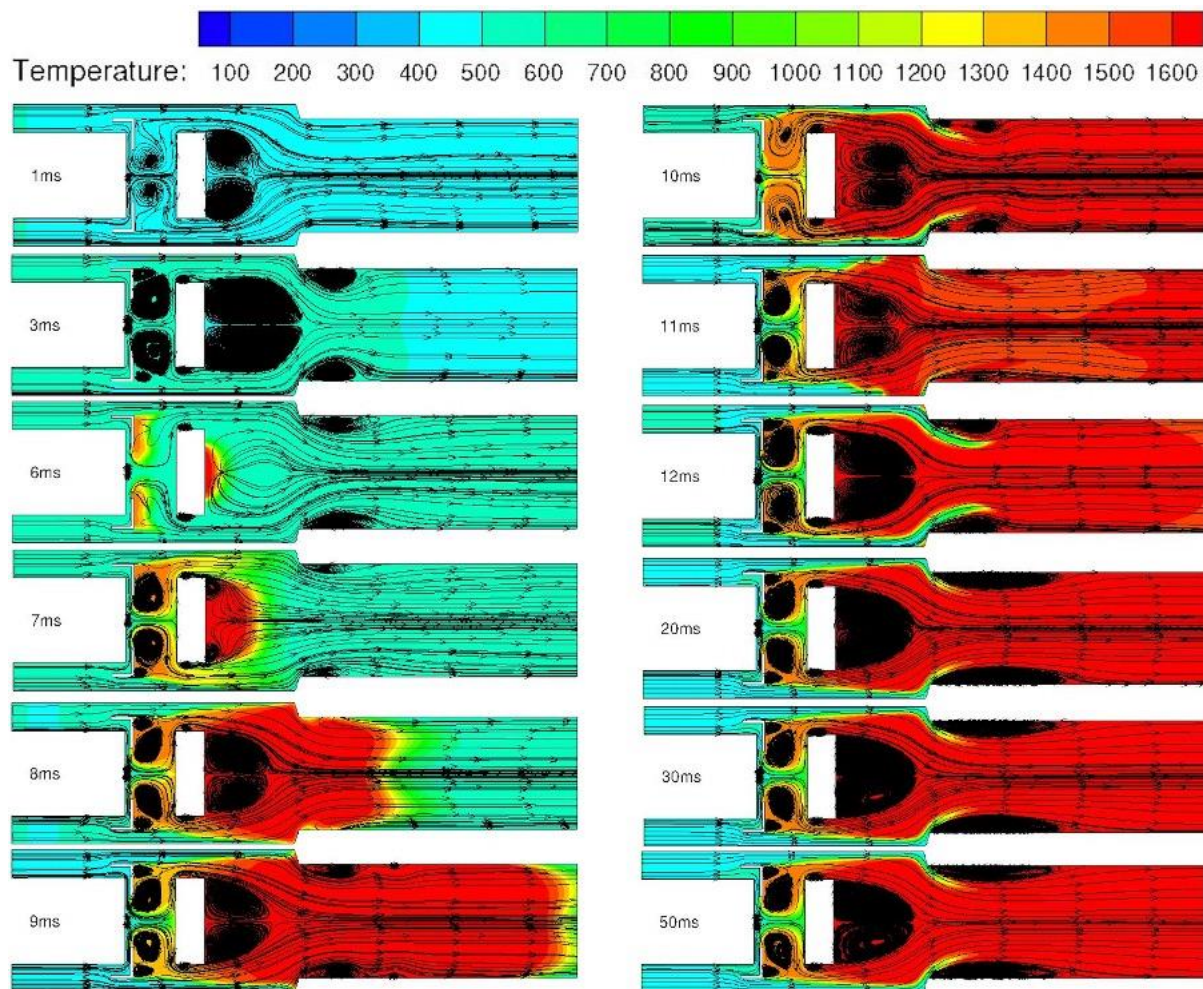


Fig. 31. Comparison between different time instant when θ is 15° .

Fig. 32 shows cases when the angle is 30. We can find that at 7ms, the couple of vortices near the wall are smaller than sharper case. The reason can be explained that the recirculation effect is slighter than the sharper cases so at 8ms, a couple of very small vortices are still existing, but in the previous two cases, they are not present at this time instant. Compared with the cases when the slope of the angle is shaper, the general temperature in this case is lower from the legend and the temperature inside the cavity is lower than previous cases compared with the zone near the outlet. In this case, shedding of vortices also is present from 9ms to 10ms but stops appearing at 11ms. From 11ms to 12ms, vortices behind the rear blunt body have a further growth and keep constant from 12ms on. The speed of the spreading of flame is slower in this configuration compared with the vertical situation.

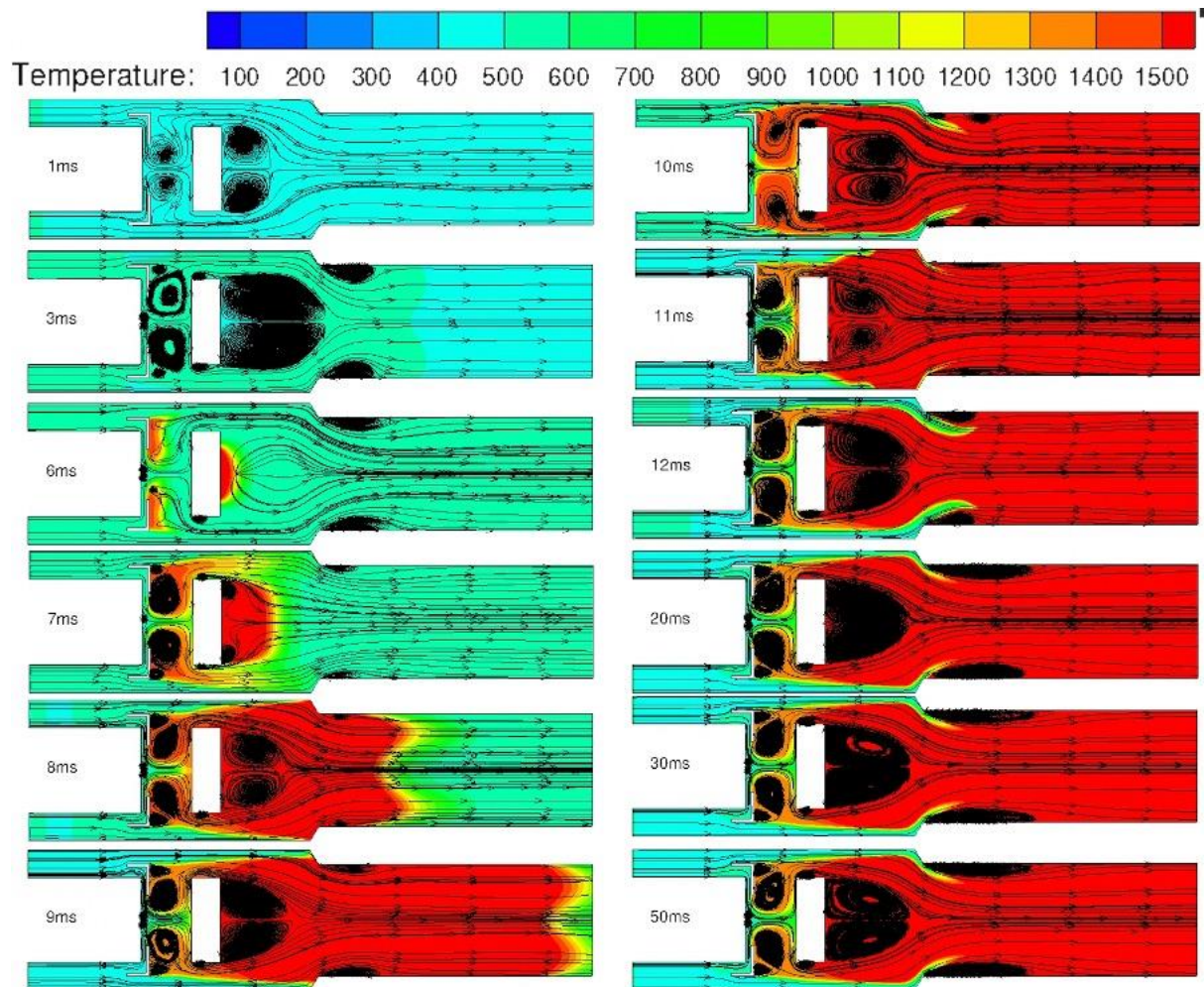


Fig. 32. Comparision between different time instant when θ is 30°.

Fig. 33 gives information about the flow and temperature field when the angle is 45°. It is found that the shape of the flame changes a lot compared with the above discussed cases. At 8ms, the shape of the flame is like a pair of scissors, and in the next step, it looks more similar, but in

the previous cases, the shape of the flame is like mountain, the distance between valley and peak is not that large. Another difference that is worth to mention is that in this case the shedding of the vortices does not appear, which indicates the good stability of this configuration.

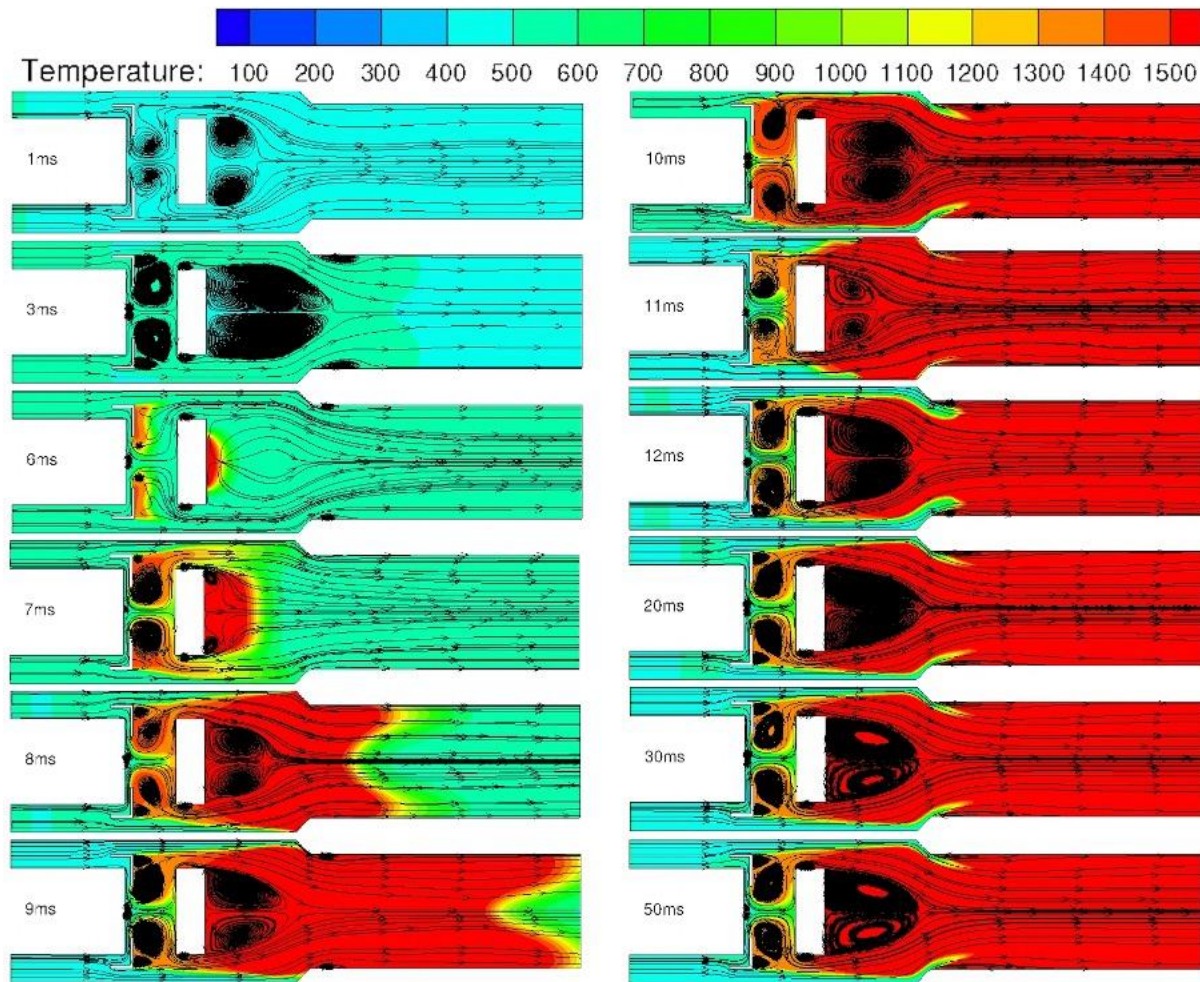


Fig. 33. Comparison between different time instant when θ is 45° .

Finally discussed is Fig. 34, which shows the changes of streamline and temperature with time. The most evident difference is that formation of the vortices near the wall is not possible due to the plain angle of inclination. Making a comparison between the temperature inside the cavity of 10ms and 50ms, we can find that the higher temperature area is reduced due to the formation of complete double-vortex structure.

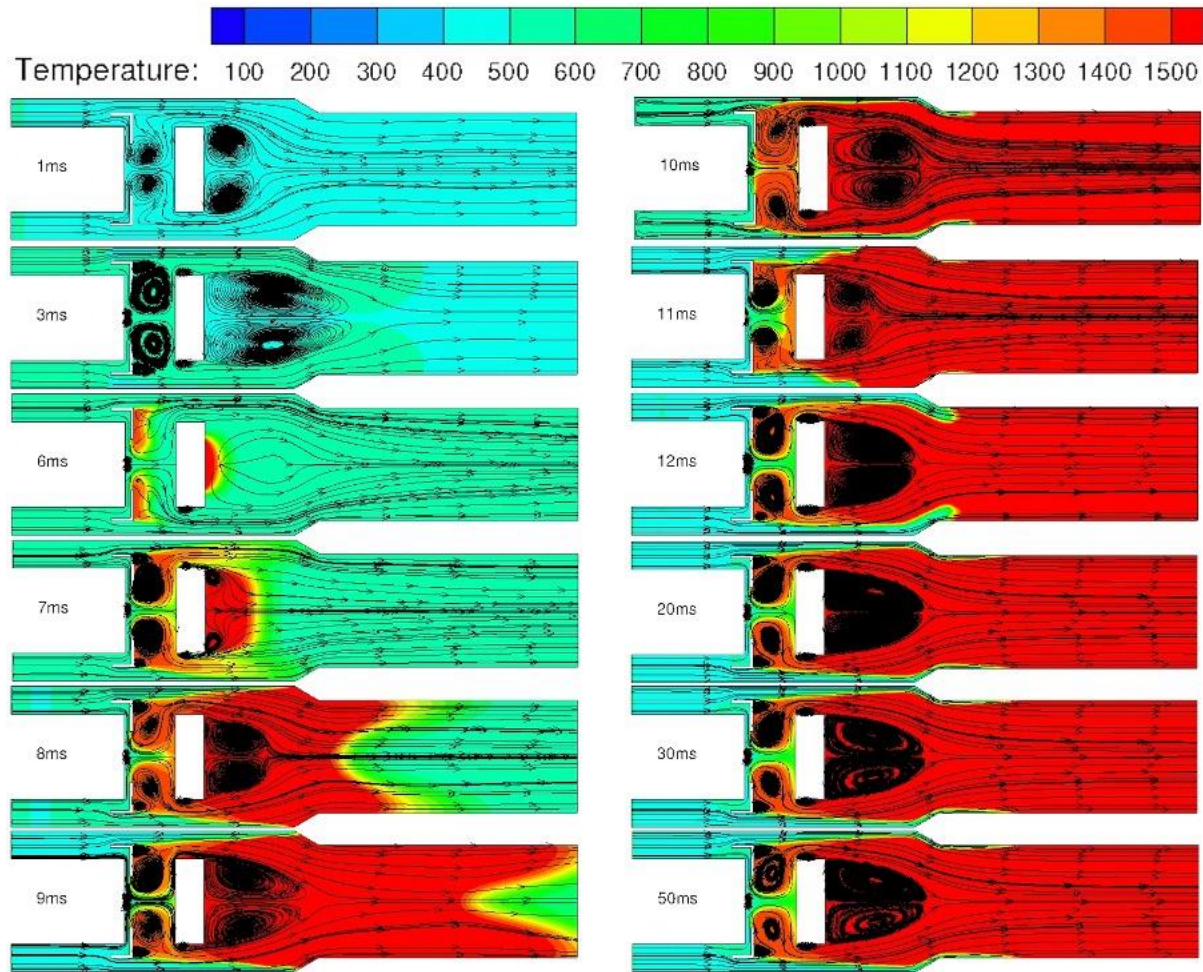


Fig. 34. Comparison between different time instant when θ is 60° .

Generally, the angle should not be too sharp with respect to horizontal direction to avoid too large pressure loss and many times of shedding of vortices.

The attention is paid to study the effects of the geometrical sizes on the performance of the combustor. 3 main groups of parameters are analyzed in instantaneous cases. The results show that the sizes have effects on the development of the vortices and flow field, and they should be chosen carefully.

5. Conclusions

This work has discussed the performance of a modified AVC model compared with its original counterpart. In this modified model, variable cross-section is designed. The parameters of the cross-section are studied. The results obtained allow us to compare the performance of the newly proposed model and to study the performance of this combustor at different structures of the convergent cross-section. The main conclusions are:

- (1) The proposed advanced vortex combustor achieves better stability of the flame and more complete combustion.
- (2) The length of the undercut has less effects on the flow and temperature field, but too large size should be avoided.
- (3) The value of l/L should not be too small to prevent pressure loss from being too large.
- (4) If the angle is sharp with respect to the horizontal level, many times of shedding of vortices would happen.

Acknowledgement

On the completion of the thesis, I would like to thank those who helped me with my graduate study and thesis during this period.

Thanks to Prof. FERLAUTO MICHELE and Prof. ZHU YUEJIN for their careful and key guidance during my thesis writing.

Thanks to the hard work of the family, thanks to the girlfriend 's considerate support and heart-warming encouragement, she is almost the source of all my motivation.

Thanks to my colleagues CUI GUIYANG, SAEID NAZARI, GUO CHAO, ZHANG XIU and other my good friends. Thanks for their two years of company with me abroad.

Thanks to all professors who have ever taught me during my graduate study.

Reference

- 1) Stowe R A, Champlain A D, Mayer A E H J. Modelling combustion performance of a ducted rocket[R], AIAA 2000 - 3728. 2000.
- 2) Ristori A, Dufor E. Numerical simulation of ducted rocket motor[R], AIAA 2001 -3193. 2001.
- 3) Agarwal K, Krishna S. & Ravikrishna R. Mixing Enhancement in a Compact Trapped Vortex Combustor[J], *Combustion Science and Technology*, 2013,185:3, 363-378.
- 4) Zeng Z, Ren J, Liu X, et al. The unsteady turbulence flow of cold and combustion case in different trapped vortex combustor[J]. *Applied Thermal Engineering*, 2015, 90: 722-732.
- 5) Kendrick D, Chenevert B, Trueblood B, Tonouchi J, Lawlor SP, Steele R. Combustion system development for the ramgen engine[J]. *J Eng Gas Turbines Power* 2003;125(4):885-94.
- 6) Edmonds RG, Steele RC, Williams JT, Straub DL, Casleton KH, Bining A. ASME 2006-GT-90319, May 2006. In: *Ultra-low NOx advanced vortex combustor power for Land, Sea, and Air[C]* 2006. ASME Turbo Expo; 2006.
- 7) Zeng ZX, Wang HY, Wang ZK. Analysis of cooling performance and combustion flow in advanced vortex combustor with guide vane[J]. *Aero Sci Technol*, 2018;72:542-52.
- 8) Hsu KY, Goss LP, Roquemore WM. Characteristics of a trapped-vortex combustor [J]. *J Propuls Power* 1998;14(1):57-65.
- 9) Stone C, Menon S. Simulation of fuel-air mixing and combustion in a trapped- vortex combustor[C]. In: *38th AIAA aerospace sciences meeting and exhibit; 2000*. paper AIAA 2000-0478.
- 10) Selvaganesh P, Vengadesan S. Cold flow analysis of trapped vortex combustor using two equation turbulence models [J]. *Aeronaut J* 2008;112(1136):569-80.
- 11) Ghenai C, Zbeeb K, Janajreh I. Combustion of alternative fuels in vortex trapped combustor [J]. *Energy Convers Manag* 2013, 65:819-28.
- 12) Agarwal K, Ravikrishna R. Experimental and numerical studies in a compact trapped vortex combustor: stability assessment and augmentation [J]. *Combust Sci Technol* 2011;183(12):1308-27.
- 13) Kumar P, Mishra D. Numerical investigation of the flow and flame structure in an axisymmetric trapped vortex combustor[J]. *Fuel*, 2012, 102 :78-84.

- 14) Wu Z, Jin Y, He X, Xue C, et al. Experimental and numerical studies on a trapped vortex combustor with different struts width[J]. *Applied Thermal Engineering*, 2015, 91:91-104.
- 15) Wu Z, He X, Jin Y, Song Y, et al. Impact of interaction between cavity flow and mainstream on the performance of a model trapped vortex combustor[J]. *Proceedings of the Institution of Mechanical Engineers, Part G: Journal of Aerospace Engineering*, 2015, 230(7), 1181-1200.
- 16) Kumar E, Kumar P, & Mishra D. Experimental investigation on the performance characteristics of a 2D trapped vortex combustor[J]. *Proceedings of the Institution of Mechanical Engineers, Part G: Journal of Aerospace Engineering*, 2016, 230(10), 1840–1847.
- 17) Vengadesan S, Sony C. Enhanced vortex stability in trapped vortex combustor[J]. *Aeronaut J* 2016;114(1155):333-7.
- 18) Krishna S, Ravikrishna R. Numerical and Experimental Studies on a Syngas-Fired Ultra Low NO_x Combustor. *ASME. J. Eng. Gas Turbines Power*. November 2017; 139(11): 111502.
- 19) Li M, He X, Zhao Y, et al. Dome structure effects on combustion performance of a trapped vortex combustor[J]. *Applied Energy*, 2017, 208:72-82.
- 20) Li M, He X, Zhao Y. Effect of strut length on combustion performance of a trapped vortex combustor[J]. *Aerospace Science and Technology*, 2018, 76:204-216.
- 21) Zhao D, Gutmark, et al. A review of cavity-based trapped vortex, ultra-compact, high-g, inter-turbine combustors[J]. *Progress in Energy and Combustion Science*, 2018, 66:42-82.
- 22) Li M, He X, Zhao Y, et al. Performance enhancement of a trapped-vortex combustor for gas turbine engines using a novel hybrid-atomizer[J]. *Applied Energy*, 2018, 216:286-295.
- 23) Zhu Y, Jin Y, He X. Effects of location and angle of primary injection on the cavity flow structure of a trapped vortex combustor model[J]. *Optik - International Journal for Light and Electron Optics*, 2019.
- 24) Ghenai C. Combustion of sustainable and renewable biohythane fuel in trapped vortex combustor[J]. *Case Studies in Thermal Engineering*, 2019, 14.
- 25) Deng YB, Jiang X, Su FM. Combustion characteristics of advanced vortex combustor burning H₂ fuel[C]. In: *ASME 2014 international mechanical engineering congress and exposition*; 2014. paper IMECE2014-37475.

- 26) Deng YB, Zheng LH, Su FM, Ma CS. Flow and combustion characteristics of annular advanced vortex combustor[C]. In: ASME 2016 international mechanical engineering congress and exposition; 2016. paper IMECE2016-65304.
- 27) Zeng ZX, Du P, Wang ZK, Li K. Combustion flow in different advanced vortex combustors with/without vortex generator[J]. Aero Sci Technol 2019; 86:640-9.
- 28) Xie J, Zhu Y. Characteristics study on a modified advanced vortex combustor[J]. Energy, 2020, 193.